VOLUME 30 NUMBER 3 July 2024
pISSN 2287-2728
eISSN 2387-285X

CLINICAL and MOLECULAR HEPATOLOGY

The forum for latest knowledge of hepatobiliary diseases

Spears and shields for liver transplantation

Sorafenib versus Lenvatinib Post-ATE/BEV in HCC
Bariatric intervention improves MASH
Non-liver cancer risk of ETV vs TDF
Dynamic changes in MASLD and HCC risk

KASL

pISSN 2287-2728
eISSN 2287-285X

CLINICAL and MOLECULAR HEPATOLOGY

https://doi.org/10.3350/cmh.2024.0107
Clinical and Molecular Hepatology 2024;30:515-538

Original Article

Macrophage ATG16L1 expression suppresses metabolic dysfunction-associated steatohepatitis progression by promoting lipophagy

Qi Wang[1,2]*, Qingfa Bu[2,3]*, Zibo Xu[2]*, Yuan Liang[2], Jinren Zhou[2], Yufeng Pan[2], Haoming Zhou[2], and Ling Lu[2,3,4]

[1]Department of General Surgery, First Affiliated Hospital of Anhui Medical University, Hefei, China; [2]Hepatobiliary Center, The First Affiliated Hospital of Nanjing Medical University, Research Unit of Liver Transplantation and Transplant Immunology, Chinese Academy of Medical Sciences, Nanjing; [3]Department of General Surgery, Nanjing BenQ Medical Center, The Affiliated BenQ Hospital of Nanjing Medical University, Nanjing; [4]Affiliated Hospital of Xuzhou Medical University, Xuzhou, China

Graphical Abstract

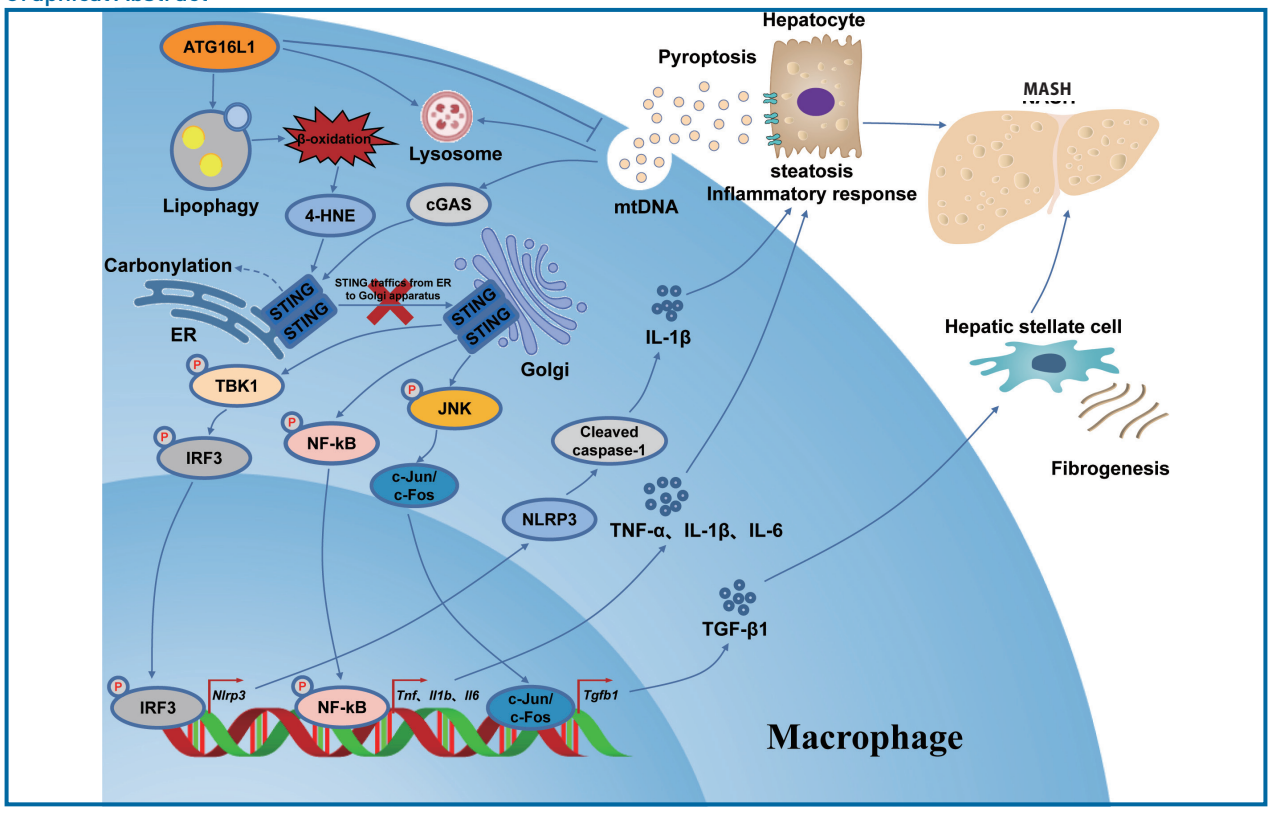

Study Highlights

- ATG16L1 expression is downregulated in liver of patients with metabolic dysfunction-associated steatohepatitis.
- Macrophage-specific *Atg16l1* knockout exacerbates and transgenic overexpression of *Atg16l1* attenuates steatohepatitis.
- Macrophage ATG16L1 suppresses steatohepatitis progression by promoting lipophagy.
- Macrophages ATG16L1 inhibit hepatocytes steatosis and HSCs activation.
- ATG16L1 may be a promising therapeutic target for MASH management.

Background/Aims: Metabolic dysfunction-associated steatohepatitis (MASH) is an unmet clinical challenge due to the rapid increased occurrence but lacking approved drugs. Autophagy-related protein 16-like 1 (ATG16L1) plays an important role in the process of autophagy, which is indispensable for proper biogenesis of the autophagosome, but its role in modulating macrophage-related inflammation and metabolism during MASH has not been documented. Here, we aimed to elucidate the role of ATG16L1 in the progression of MASH.

Methods: Expression analysis was performed with liver samples from human and mice. MASH models were induced in myeloid-specific *Atg16l1*-deficient and myeloid-specific *Atg16l1*-overexpressed mice by high-fat and high-cholesterol diet or methionine- and choline-deficient diet to explore the function and mechanism of macrophage ATG16L1 in MASH.

Results: Macrophage-specific *Atg16l1* knockout exacerbated MASH and inhibited energy expenditure, whereas macrophage-specific *Atg16l1* transgenic overexpression attenuated MASH and promotes energy expenditure. Mechanistically, *Atg16l1* knockout inhibited macrophage lipophagy, thereby suppressing macrophage β-oxidation and decreasing the production of 4-hydroxynonenal, which further inhibited stimulator of interferon genes (STING) carbonylation. STING palmitoylation was enhanced, STING trafficking from the endoplasmic reticulum to the Golgi was promoted, and downstream STING signaling was activated, promoting proinflammatory and profibrotic cytokines secretion, resulting in hepatic steatosis and hepatic stellate cells activation. Moreover, *Atg16l1*-deficiency enhanced macrophage phagosome ability but inhibited lysosome formation, engulfing mtDNA released by pyroptotic hepatocytes. Increased mtDNA promoted cGAS/STING signaling activation. Moreover, pharmacological promotion of ATG16L1 substantially blocked MASH progression.

Conclusions: ATG16L1 suppresses MASH progression by maintaining macrophage lipophagy, restraining liver inflammation, and may be a promising therapeutic target for MASH management. **(Clin Mol Hepatol 2024;30:515-538)**

Keywords: ATG16L1; Macrophages; Lipophagy; Metabolic dysfunction-associated steatohepatitis

Corresponding author : **Ling Lu**
Hepatobiliary Center, The First Affiliated Hospital of Nanjing Medical University, 300 Guang Zhou Road, Nanjing, 210029, Jiangsu, China
Tel: +86-25-68033934, Fax: +86-25-83718836, E-mail: lvling@njmu.edu.cn
https://orcid.org/0000-0002-4983-5557

Haoming Zhou
Hepatobiliary Center, The First Affiliated Hospital of Nanjing Medical University, 300 Guang Zhou Road, Nanjing, 210029, Jiangsu, China
Tel: +86-25-68303947, Fax: +86-25-68136450, E-mail: hmzhou@njmu.edu.cn
https://orcid.org/0000-0003-2778-221X

*These authors contributed equally to this paper.

Editor: Sungsoon Fang, Yonsei University College of Medicine, Korea

Received : Feb. 13, 2024 / **Revised :** Apr. 28, 2024 / **Accepted :** May. 10, 2024

Abbreviations:

MASH, metabolic dysfunction-associated steatohepatitis; ATG16L1, autophagy-related protein 16-like 1; 4-HNE, 4-hydroxynonenal; HSCs, hepatic stellate cells; HFHCD, high-fat and high-cholesterol diet; MCD, methionine- and choline-deficient diet; ***Atg16l1*$^{\Delta Mf}$**, myeloid-specific ***Atg16l1*** knockout; ***Atg16l1*$^{\Delta Mf}$*Tmem173*$^{\Delta Mf}$**, myeloid-specific ***Atg16l1*** and ***Tmem173*** double knockout; ***Atg16l1*^{OE}**, myeloid-specific ***Atg16l1-overexpressing*** knockin; BMDMs, bone marrow-derived macrophages; BAT, brown adipose tissue; eWAT, epididymal white adipose tissue; ingWAT, inguinal white adipose tissue; EE, energy expenditure; CM, conditioned media; TG, hepatic triglyceride; ERGIC, endoplasmic reticulum–Golgi intermediate complex; TBK1, TANK-binding kinase 1; IRF3, interferon regulatory factor 3; ER, endoplasmic reticulum; GSDMD, Gasdermin D; mtDNA, mitochondrial DNA; STING, stimulator of interferon genes

INTRODUCTION

Metabolic dysfunction-associated steatotic liver disease (MASLD) is emerging as the leading chronic liver disease worldwide.[1,2] The more advanced subtype, metabolic dysfunction-associated steatohepatitis (MASH), characterized by hepatic steatosis, lobular inflammation, and ballooning with or without perisinusoidal fibrosis,[3] conveys progressive liver injury that can lead to cirrhosis and hepatocellular carcinoma.[4] The majority of MASLD cases are heterogeneous, asymptomatic, and not easily identifiable, even when the disease has progressed to cirrhosis.[5] Currently, treatment options for MASH are extremely limited; the only proven treatments are weight loss and increased physical activity, which are difficult to sustain; there is still a lack of approved pharmacotherapies for this medical condition.[5,6] Thus, more studies are needed to identify key molecular regulators of MASH progression and to lay the foundation for developing effective therapeutic treatments.

Autophagy is a conserved catabolic pathway in eukaryotic cells that is essential for survival, development, and homeostasis, in which the lysosome is the end point for components to be phagocytosed.[7-9] Autophagy in hepatic macrophages protects the liver against fibrosis,[10,11] especially during experimental alcoholic injury or MASH.[12] One of the main functions of autophagy is to regulate cellular metabolism and energy through lipophagy, mitophagy, refueling of the amino acid pool, or degradation of proteins involved in glucose metabolism.[13,14] ATG16L1 plays an important role in the process of autophagy and mediates the conjugation of phosphatidylethanolamine to the ubiquitin-like molecule LC3—a necessary step for proper biogenesis of the autophagosome and for subsequent events in which substrates are degraded by the lysosome.[15] A study indicated that disrupted ATG16L1 activity in hepatocytes impaired hepatocyte lipophagy during hepatic steatosis.[16] Nevertheless, the specific role of ATG16L1 in macrophages in regulating hepatic inflammation, fibrosis, and lipid metabolism disturbance during MASH remains unclear.

Therefore, our study aimed to elucidate the role of macrophage ATG16L1 in regulating hepatic inflammation, fibrosis, and lipid metabolism disturbance during MASH. By investigating the expression and function of ATG16L1 in macrophages, we sought to uncover novel insights into the pathogenesis of MASH and to explore potential genetic-based strategies for its treatment. The elucidation of the precise mechanisms by which ATG16L1 influences MASH progression is of paramount importance, as it may influence the development of targeted therapies that address the underlying molecular dysregulation. This, in turn, holds the potential to significantly improve outcomes for MASH patients, inhibiting the progression of MASH to advanced stages such as cirrhosis and hepatocellular carcinoma. Furthermore, our findings may contribute to a broader understanding of autophagy-mediated processes in liver health and disease, providing a basis for future research endeavors aiming at unraveling the intricate interplay between cellular pathways and disease pathogenesis.

MATERIALS AND METHODS

Human liver samples

Human liver samples were collected from 39 patients with MASH (39 frozen tissues for mRNA expression detection and 6 paraffin-embedded slides for protein expression detection), and 31 patients without hepatic steatosis (patients who presented with hepatic hemangioma at the First Affiliated Hospital of Nanjing Medical University) were used as controls (Supplementary Table 1). Individuals in the control group had no history of diabetes, alcohol use, viral hepatitis, or other liver diseases. All liver specimens were assessed independently by two experienced pathologists blinded to the NAFLD activity score (NAS) clinical data, which is defined as the sum of steatosis, inflammation, and hepatocyte ballooning scores. Patients with an NAS ≥5 were considered likely to have MASH. The clinical characteristics of the patients with MASH are listed in Supplementary Table 1. The study was approved by the Institutional Ethics Committee of the First Affiliated Hospital of Nanjing Medical University (approval number: 2020-SRFA-288). Informed consent for tissue analysis was obtained before liver biopsy or surgery. All experiments were performed in accordance with government policies and the Declaration of Helsinki and Istanbul.

Animals and treatments

Wild-type (WT), FloxP-Atg16l1 (Atg16l1$^{fl/fl}$), Lyz2-Cre At-

g16l1-knockout (Atg16l1$^{\Delta M\phi}$), Lyz2-Cre Atg16l1 and Lyz2-Cre Tmem173-double knockout (Atg16l1$^{\Delta M\phi}$Tmem173$^{\Delta M\phi}$), and myeloid-specific Atg16l1-overexpressing-knockin (Atg16l1^{OE}) male mice, 6–8 weeks old, on a C57BL/6 background were used in the experiments (Supplementary Table 2). Mice were randomly assigned to receive a normal chow diet (NCD), a high-fat and high-cholesterol diet (HFHCD) (Research Diets, Inc., New Brunswick, CA, USA) for 16 weeks (n=6–8 per group), or a methionine- and choline-deficient (MCD) diet (Research Diets, Inc.) for 6 weeks (n=6–8 per group). Male wild-type C57BL/6 mice (6–8 weeks old) were administered the ATG16L1 enhancer peretinoin (0.03% for 16 consecutive weeks or 6 consecutive weeks) in the diet,[17] or vehicle (saline) for 16 weeks of HFHCD feeding or for 6 weeks of MCD feeding (n=6–8 per group). All the mice were housed under specific pathogen-free, ventilated, thermostatic conditions with a 12-hours light/dark cycle at 24°C. Food intake was measured over one week using racks in a regular cage that were weighed every day, and daily food intake was calculated as kcal/day within the indicated period. The mice were fasted at the end of the experiments. Finally, serum and tissues were harvested as described in our previous study.[18] The livers and adipose tissues were rapidly excised and weighed. All animal studies were performed according to the guidelines of the Institutional Animal Use and the Animal Experimentation Ethics Committee of The First Affiliated Hospital of Nanjing Medical University.

Cell culture and treatment

Primary hepatocytes were isolated from male *Atg16l1*$^{fl/fl}$ or WT mice as previously described.[19] The liver macrophage pellet was resuspended and cultured. Cells were treated with a mixture of palmitic acid (PA; 0.5 mM; Sigma-Aldrich) and oleic acid (OA; 1.0 mM; Sigma-Aldrich) coupled with bovine serum albumin (BSA; Sigma-Aldrich) for the indicated periods. BSA was used as a vehicle control. Bone marrow cells were isolated from the femurs and tibias of male *Atg16l1*$^{\Delta M\phi}$, *Atg16l1*^{OE}, and *Atg16l1*$^{fl/fl}$ mice. The bone marrow was flushed with DMEM loaded into a 1 mL syringe. Bone marrow cells were cultured at a concentration of 3×10^6/mL in DMEM supplemented with 10% FBS and 20% L929 conditioned medium to differentiate them into bone marrow-derived macrophages (BMDMs). On day 7, all adherent cells differentiated into mature macrophages.

For coculture studies, primary hepatocytes from male *Atg16l1*$^{fl/fl}$ mice and LPS-primed (10 ng/mL of LPS for 4 hours) macrophages[20] from the bone marrow of male *Atg16l1*$^{\Delta M\phi}$, *Atg16l1*^{OE}, or *Atg16l1*$^{fl/fl}$ mice were seeded in a coculture chamber (Corning Inc., Corning, NY, USA). The coculture system was supplemented with palmitic acid and oleic acid media. Mouse TNF-α-neutralizing mAb (10 ng/mL) (CST, Danvers, MA, USA), MR16-1 (12.5 ng/mL) (Chugai Pharmaceutical, Shizuoka, Japan), IL-1RA (12.5 ng/mL) (MedChemExpress, Princeton, NJ, USA), TNF-α (10 ng/mL), IL-6 (12.5 ng/mL), or IL-1β (12.5 ng/mL) (Novus Biologicals, Littleton, CO, USA) was added to the coculture system for 24 hours, and the hepatocytes were subsequently analyzed for fat accumulation and inflammatory response indices. LPS-primed (10 ng/mL LPS for 4 hours) BMDMs were incubated with hepatocyte-CM for 48 hours and subjected to RNA sequencing analysis. Primary mouse HSCs were isolated as previously described.[21] Briefly, primary hepatic stellate cells (HSCs) were isolated from the livers of mice. After portal vein intubation, the livers were perfused in situ with Ca^{2+}-free Hank's balanced saline solution (HBSS) at 37°C for 15 minutes and subsequently perfused with the solution containing 0.05% collagenase and Ca^{2+} for 15 minutes at a flow rate of 10 mL/min. The perfused livers were minced, filtered through a 70 M cell strainer (BD Bioscience), and centrifuged at 50 × *g* for 3 minutes. The supernatant was further centrifuged at 500 × g for 10 minutes, resuspended in Ficoll plus Percoll (1:10, GE Healthcare), and centrifuged at 1,400 × *g* for 17 minutes. The HSCs were collected from the interface. Primary mouse HSCs were incubated with BMDM-CM in the absence or presence of TGF-β1 (8 ng/mL for 24 hours) and analyzed for HSC activation status.

Histological examination

H&E-stained liver sections were assessed by two experienced liver pathologists who were blinded to experimental grouping, and each liver specimen was evaluated for the presence or absence of MASH according to histopathology and for the NAFLD activity score (NAS), defined as the sum of steatosis, inflammation, and hepatocyte ballooning scores. Patients with an NAS of ≥5 were considered likely

https://doi.org/10.3350/cmh.2024.0107

to have MASH.[3,22] For oil red O staining, primary hepatocytes and frozen liver sections (10 μm) were rinsed with 60% isopropanol and stained with oil red O solution (Sigma–Aldrich) for 15 minutes. Afterward, the sections were rinsed again with 60% isopropanol, and the nuclei were stained with hematoxylin before microscopic analysis.

Biochemical assays

The serum levels of alanine aminotransferase (ALT) and aspartate aminotransferase (AST) were determined using an automated chemical analyzer (Olympus, Tokyo, Japan). Hepatic triglyceride (TG) levels were determined with a Wako E-test triglyceride kit (Wako Pure Chemical Industries, Osaka, Japan). Cellular TG synthesis was determined using standard methods.[23] Briefly, cellular lipids were extracted with hexane/isopropanol (3:2). Lipids were then dried with nitrogen gas, redissolved in chloroform, and resolved by thin-layer chromatography using successive solvent systems containing chloroform, acetone, methanol, acetic acid, and water at a volumetric ratio of 10:4:2:2:1, as well as hexane, methanol, and acetic acid at a volumetric ratio of 80:20:1. Phosphor images were obtained with a Storm Gel and Blot Imaging System (GE Healthcare).

Fatty acid β-oxidation assay

The rates of fatty acid β-oxidation were determined using a modification of a previously used method[24] that measured the rate of carbon dioxide production. Carbon dioxide trapped for 1 hour at 37°C from stimulated cells was released onto filter paper soaked in 100 mM sodium hydroxide. The rate of β-oxidation was calculated as the amount of trapped carbon dioxide in relative units produced per mg protein per hour.

Immunohistochemical and immunofluorescence staining

Murine liver and adipose tissue immunohistochemistry was performed to detect F4/80 expression in paraffin-embedded liver biopsies using an anti-F4/80 antibody (#70076, CST). Immunohistochemistry of the murine liver was performed to detect GSDMD expression in paraffin-embedded human liver biopsies using an anti-GSDMD antibody (#AF4012, Affinity). In brief, liver sections were preblocked for 10 minutes after deparaffinization. The slides were then heated in an autoclave with sodium citrate for antigen retrieval, covered in 1% hydrogen peroxide to eliminate endogenous peroxidase activity, and blocked with 2% goat serum. The slides were then incubated with primary antibodies at 4°C overnight. Biotinylated goat anti-rabbit IgG (Vector, Burlingame, CA, USA) was used as the secondary antibody, followed by incubation with immunoperoxidase (ABC Kit; Vector) according to the manufacturer's protocol. ATG16L1 and CD68 expression in human liver tissues were determined by immunofluorescence with an anti-rabbit ATG16L1 mAb (#8089, CST) and an anti-mouse CD68 mAb (ab955, Abcam), followed by incubation with secondary goat anti-rabbit IgG (ab150088, Abcam) or goat anti-mouse IgG (ab150117, Abcam). The cells were fixed using 3% paraformaldehyde and subsequently blocked and incubated with primary and corresponding Cy5- and Texas Red-conjugated secondary antibodies. Lipid droplets (LDs) were stained by incubating cells with BODIPY 493/503 (D2191, Invitrogen) for 30 minutes. The cells were then fixed and processed for immunofluorescence as previously described.[25] STING, α-SMA, LAMP1, LC3B, and GM130 expression in cells was determined by immunofluorescence using an anti-rabbit STING pAb (PA5-116052, Invitrogen), an anti-rabbit α-SMA mAb (#19245, CST), an anti-rabbit LAMP1 mAb (#99437, CST), an anti-rabbit LC3B mAb (#43566, CST), and an anti-mouse GM130 mAb (sc-55591, Santa Cruz Biotechnology), followed by incubation with secondary goat anti-rabbit IgG (ab150088, Abcam) or anti-mouse IgG (ab150117, Abcam). DAPI was used to stain the nuclei. The slides were washed twice with PBS and observed via confocal microscopy (Zeiss, Oberkochen, Germany) according to the manufacturer's protocol.

Cell transfection

A *c-Jun* adenoviral vector was constructed by GenePharma (Shanghai, China) to overexpress c-Jun in primary macrophages isolated from bone marrow. Targeted cells (2×10^5) were infected with 1×10^6 adenovirus-transducing units in the presence of 1 mg/mL polybrene. Total RNA or proteins were prepared 48 hours after transfection. Negative control adenoviral plasmid vectors were generated and

designated “Ad-Con.” Transfection of cells was performed using Lipofectamine 3000 Transfection Reagent (Thermo Fisher Scientific, Waltham, MA, USA) according to the manufacturer’s instructions, and the transfection efficiency was validated by qPCR.

Reagents

The STING inhibitor C-176, the STING activator DMXAA, the JNK activator anisomycin, the JNK inhibitor SP600125, the autophagy inhibitor 3-methyladenine (3-MA), the lipid peroxidation end product 4-hydroxynonenal (4-HNE), the β-oxidation inhibitor etomoxir, the ATG16L1 enhancer peretinoin were purchased from MedChemExpress, and the lysosomal acid lipase (LIPA) inhibitor lalistat was purchased from Enamine. All mice were euthanized for further analysis after being fed a HFHCD for 16 weeks or an MCD for 6 weeks.

RNA extraction and quantitative polymerase chain reaction (qPCR)

Total mRNA was isolated from liver samples or cells using TRIzol reagent (Invitrogen, Carlsbad, CA, USA) and reverse transcribed using a high-capacity cDNA reverse transcription kit (Roche, Indianapolis, IN, USA) according to the manufacturer’s protocols. The mRNA expression levels were quantified by quantitative PCR using SYBR Green (Roche). The expression level of each cDNA relative to that of the β-actin endogenous control was determined using the $2^{-\Delta\Delta Ct}$ method. Quantitative real-time PCR was repeated three times for each sample. The primers used in our study are listed in Supplementary Table 3.

mtDNA isolation and quantification

DNA was extracted from 200 μL of cell culture supernatant from untreated and treated primary murine hepatocytes using a QIAmp DNA Mini Kit (QIAGEN, Duesseldorf, Germany) according to the manufacturer’s instructions. Real-time polymerase chain reaction (qPCR) was performed for the quantification of mtDNA. mtDNA was quantified using mouse mt-ATP6 primers/TaqMan 5' FAM-3' MGB probes (Bio-Rad, Hercules, CA, USA). The mitochondrial lysates of primary hepatocytes were used to isolate mtDNA using a mitochondrial DNA isolation kit (Abcam) according to the manufacturer’s instructions. Total DNA was isolated using a DNeasy Blood and Tissue Kit (QIAGEN) following the manufacturer’s instructions. RT–qPCR analysis was performed using a sequence detection system (ABI Prism 7000; Applied Biosystems, Foster City, CA, USA) with a SYBR Green 1-step kit (Invitrogen). To evaluate the possibility of BMDMs engulfing mtDNA released from hepatocytes, mtDNA isolated from primary murine hepatocytes was tagged with Cy5-dCTP (Amersham Cy5-dCTP, GE Healthcare) using PCR following the manufacturer’s protocol (BioPrime DNA Labeling system, Life Technologies). The Cy5-labeled DNA PCR product was cleaned using a DNeasy Mini Spin Column (QIAGEN) before the DNA concentration was measured using a Nanodrop (Thermo Scientific).

Protein extraction and Western blotting

Whole-cell lysates were obtained as previously described.[18] Proteins in tissues or cells were extracted with ice-cold lysis buffer (0.5% sodium deoxycholate, 1% Triton X-100, 10% glycerol, 0.1% SDS, 137 mM sodium chloride, 20 mM Tris, and pH 7.4). Proteins (20 g) were separated by 12% SDS–PAGE and transferred to PVDF nitrocellulose membranes. Western blot analysis was performed using the following antibodies: anti-ATG16L1 (#8089, CST), anti-β-actin (#4970, CST), anti-α-SMA (#19245, CST), anti-collagen I (#72026, CST), anti-TIMP1 (#8946, CST), anti-p-p65 (Ser536) (ab76302, Abcam), anti-p65 (66535-1-Ig, Proteintech), anti-p-IkBα (#2859, CST), anti-IkBα (10268-1-AP, Proteintech), anti-TNF-α (60291-1-Ig, Proteintech), anti-IL-6 (66146-1-Ig, Proteintech), anti-cleaved IL-1β (#63124, CST), anti-pro-IL-1β (#12242, CST), anti-cGAS (#79978, CST), anti-STING (#13647, CST), anti-p-TBK1 (#5483, CST), anti-TBK1 (#38066, CST), anti-p-IRF3 (#37829, CST), anti-IRF3 (ab68481, Abcam), anti-NLRP3 (#15101, CST), anti-cleaved caspase-1 (#89332, CST), anti-pro-caspase-1 (#24232, CST), anti-p-JNK (#9255, CST), anti-JNK (#9252, CST), anti-c-Jun (#9165, CST), anti-c-Fos (#74620, CST), anti-LC3B (#43566, CST), anti-p62 (#5114, CST), anti-GSDMD (#AF4012, Affinity), anti-rabbit IgG (#7074, CST), and anti-mouse IgG (#7076, CST). Image Lab software (National Institutes of Health) was used to quantify the protein expression, and β-actin was the con-

https://doi.org/10.3350/cmh.2024.0107

trol.

In vitro carbonylation

STING protein was expressed using a TNT Quick Coupled Transcription/Translation System (Promega) according to the manufacturer's instructions.[26] STING protein was incubated with 100 μM FeSO4/25 mM ascorbate and 25 mM H_2O_2 in 100 mM KCl, 100 mM $MgCl_2$, and 50 mM HEPES (pH 7.2), and the reaction proceeded for 5 hours.[27] To remove excess low-molecular-weight compounds, proteins were concentrated with an Amicon Ultra 10 kDa filter (Millipore). STING carbonylation was evaluated using OxyBlot technology.

Validation of protein palmitoylation by click chemistry

BMDMs were incubated with 100 μM palmitic acid probes (Invitrogen C10265) for 4 hours at 37°C. The cells were washed twice in PBS and then lysed on ice in 100 μL of 50 mM Tris, pH 8.0, containing 0.4% SDS and protease inhibitors, and the lysate was incubated with 1 mM CuSO4, 100 μM TBTA ligands, 100 μM biotin-alkyne, and 1 mM tris(2-carboxyethyl) phosphine for 1 hour at 25°C. After precipitation, protein complexes were enriched by adding streptavidin beads for 3 hours. Samples were washed three times with PBS, and SDS loading buffer was used to elute proteins at 95°C for 20 minutes, after which SDS–PAGE was used to separate the proteins.

DNA pull-down assay

An *in vitro* pull-down assay was performed to detect the binding of c-Jun and c-Fos to *Tgfb1*. BMDMs were lysed in NP-40 lysis buffer. Lysates were incubated with biotin-c-Jun or c-Fos (BioLog Life Science Institute) at 4°C for 4 hours and then incubated with streptavidin beads at 4°C for 4 hours. The beads were washed four times with lysis buffer and analyzed for *Tgfb1* binding by immunoblotting.

Chromatin immunoprecipitation (ChIP) assays

The ChIP assay was performed using a Simplechip Enzymatic Chromatin IP Kit (Cell Signaling Technology, Billerica, MA, USA) according to the manufacturer's instructions. Briefly, the cells were cross-linked with 37% formaldehyde, and the nuclei were subsequently extracted. After fragmentation by sonication and enzymatic digestion, the DNA–protein complex was subjected to immunoprecipitation with 8 μg of anti-c-Jun antibody (Cell Signaling Technology) or rabbit IgG as a control. Purified ChIP DNA was amplified by real-time quantitative PCR. The primers for the AP-1 region of the *Tgfb1* promoter were as follows: forward, 5'-GAAGGGGAGAGATGGCTCCACTGGG-3'; reverse, 5'-CTCCTCCTCATGGACTTGCTTT-3'.

Luciferase assays

A *Tgfb1* promoter luciferase reporter plasmid (*Tgfb1* luciferase) was constructed using a pGL3 luciferase vector (Promega, WI) according to the manufacturer's instructions. BMDMs were transfected with the pGL3-*Tgfb1*-luciferase vector. After transfection for 6 h, the cells were washed and transfected with Ad-*c-Jun* or Ad-Con. After 48 h, the cells were lysed with passive lysis buffer, and transcriptional activity was measured using a luciferase assay system (Promega) according to the manufacturer's instructions.

Indirect calorimetry

VO_2, VCO_2, the respiratory exchange ratio (RER), and locomotor activity were assessed using an eight-chamber Oxymax system (Columbus Instruments).[3] Mice were placed in the chambers at 23°C with free access to food and water and acclimated for more than 50 minutes before measurement. Energy expenditure (EE) was calculated as $(3.815+1.232\times RER)\times VO_2$/lean mass.

Electron microscopy

Primary hepatocytes were immersed in fixative (2.5% glutaraldehyde) and stored overnight at 4°C. The samples were rinsed in the same buffer and postfixed for 1 h in 1% osmium tetroxide and 1% potassium ferrocyanide in 0.1 M cacodylate buffer to enhance membrane staining. The cells were then rinsed in distilled water, dehydrated in acetone at a low temperature to preserve lipids, and embedded in epoxy resin. Contrasted ultrathin sections (70 nm) were ana-

lyzed under a transmission electron microscope (HITACHI, Tokyo, Japan).

RNA sequencing and analysis

LPS-primed *Atg16l1*$^{fl/fl}$ or *Atg16l1*$^{\Delta M\phi}$ BMDMs were incubated with *Atg16l1*$^{fl/fl}$ primary hepatocyte-conditioned media (CM) for 48 h, and *Atg16l1*$^{fl/fl}$ or *Atg16l1*$^{\Delta M\phi}$ BMDMs were subsequently subjected to RNA sequencing analysis (n=3/group). Total RNA was extracted from cells using TRIzol reagent (Invitrogen). cDNA libraries were constructed for each pooled RNA sample using the NEBNext® Ultra™ RNA Library Prep Kit for Illumina® (NEB, Ipswich, MA, USA) according to the manufacturer's instructions. Pathway analysis was used to determine the pathways significantly associated with DEGs according to the KEGG database.

Enzyme-linked immunosorbent assay (ELISA)

The serum and media levels of the cytokines TNF-α, IL-6, IL-1β (Thermo Fisher Scientific), and 4-HNE (MyBioSource) were determined using ELISA kits according to the manufacturer's instructions.

Statistical analysis

All the data were analyzed using unpaired Student's t tests or one-way ANOVA accompanied by Bonferroni post hoc t tests. Statistical significance was set at $P \leq 0.05$ (two-tailed). Statistical analysis was performed using GraphPad Prism Version 7.0 software (GraphPad Software, San Diego, CA, USA).

RESULTS

ATG16L1 expression is downregulated in livers of patients with MASH, and macrophage deficiency of ATG16L1 expression exacerbates steatohepatitis development.

To investigate the involvement of ATG16L1 in MASH progression, we examined *ATG16L1* expression in liver tissues from 39 patients with MASH and 31 without steatosis (Supplementary Table 1). The liver tissues were subjected to H&E and oil red O staining (Fig. 1A). The results showed that *ATG16L1* gene expression and ATG16L1 protein expression were significantly lower in MASH patients than in normal controls (Fig. 1B, C). Furthermore, hepatic *ATG16L1* expression levels were negatively correlated with the levels of serum transaminases (ALT and AST) and hepatic inflammation indicators (*TNFA*, *IL6*, and *IL1B*) (Fig. 1D, E). Dual-immunofluorescence staining of liver sections with the human macrophage marker CD68 showed that ATG16L1 expression was markedly inhibited in macrophages in the livers of patients with MASH (Fig. 1F). To further confirm these findings, murine MASH models were generated via HFHCD feeding for 16 weeks or MCD feeding for 6 weeks (Supplementary Fig. 1A–D). Analysis revealed that hepatic *Atg16l1* gene expression and ATG16L1 protein expression were significantly lower in MASH mice than in normal controls (Fig. 1G, H). Because macrophage infiltration is implicated in this process, we assessed the effect of macrophage ATG16L1 expression on the progression of steatohepatitis. We generated *Lyz2-Cre Atg16l1*-knockout (*Atg16l1*$^{\Delta M\phi}$) mice. The overall expression levels of ATG16L1 in liver tissues or hepatocytes from *Atg16l1*$^{\Delta M\phi}$ and *Atg16l1*$^{fl/fl}$ mice showed no significant difference. BMDMs isolated from *Atg16l1*$^{\Delta M\phi}$ mice showed ATG16L1 knockout compared to those isolated from *Atg16l1*$^{fl/fl}$ mice (Supplementary Fig. 1E). *Atg16l1*$^{\Delta M\phi}$ mice and *Atg16l1*$^{fl/fl}$ mice were bred and fed an NCD or an HFHCD for 16 weeks. The results demonstrated that macrophage *Atg16l1* knockout increased proinflammatory gene expression and macrophage infiltration (Supplementary Fig. 1F, G). Histopathology of liver sections demonstrated that *Atg16l1*$^{\Delta M\phi}$ mice had exacerbated injury and significantly more steatosis and inflammation than did *Atg16l1*$^{fl/fl}$ mice fed an HFHCD or MCD (Fig. 1I). Accordingly, the serum ALT and hepatic triglyceride (TG) levels were significantly greater in the *Atg16l1*$^{\Delta M\phi}$ mice than in the *Atg16l1*$^{fl/fl}$ mice (Fig. 1J). Moreover, *Atg16l1*$^{\Delta M\phi}$ mice exhibited significantly exacerbated liver fibrosis, as indicated by increased Sirius red and α-SMA staining (Fig. 1I); increased expression levels of the profibrotic genes *Acta2*, *Col1a1*, and *Timp1*; and increased protein expression levels of α-SMA, collagen-I, and TIMP-1 (Supplementary Fig. 1H, I). The weights of tissues including livers, brown adipose tissue (BAT), epididymal WAT (eWAT), and inguinal white adipose tissue (ingWAT) of the *Atg16l1*$^{\Delta M\phi}$ mice fed an HFHCD were greater than those of the *Atg16l1*$^{fl/fl}$ mice fed the same diet

https://doi.org/10.3350/cmh.2024.0107

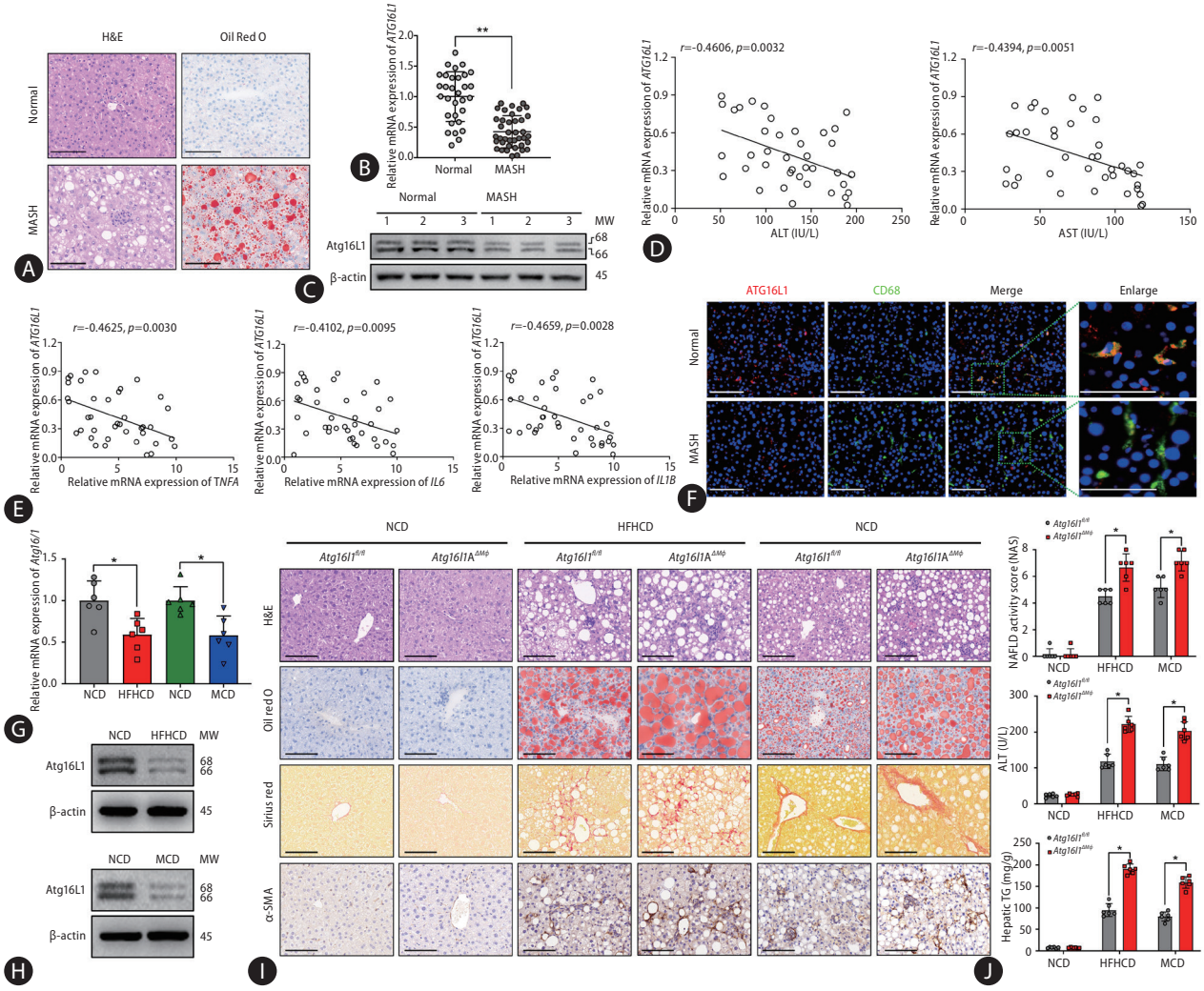

Figure 1. ATG16L1 expression is downregulated in livers of MASH patients, and macrophage *Atg16l1* knockout exacerbates the development of experimental steatohepatitis. (A) Representative H&E staining and oil red O staining (400×) of human liver tissues; n=6/group. (B) *ATG16L1* mRNA expression levels in liver tissues from patients with MASH (n=39) and without MASH (n=31). (C) ATG16L1 protein expression levels in human liver tissues. (D, E) Graphs showing the correlation between the mRNA expression levels of *ATG16L1* and the serum levels of ALT, AST and hepatic *TNFA*, *IL6*, and *IL1B* in MASH patients (n=39). (F) Dual immunofluorescence staining for CD68 and ATG16L1 (400×) expression in human liver tissues. (G) Hepatic *Atg16l1* mRNA expression levels in MASH mice. n=6/group. (H) Hepatic ATG16L1 protein expression levels in MASH mice. (I) Representative hepatic H&E staining, oil red O staining, Sirius Red staining, and α-SMA immunohistochemical analysis in MASH mice. (J) NAS, serum ALT levels, and hepatic TG levels in MASH mice; n=6/group. MASH, metabolic dysfunction-associated steatohepatitis; ATG16L1, autophagy-related protein 16-like 1; ALT, alanine aminotransferase; AST, aspartate aminotransferase; NAS, NAFLD activity score; TG, hepatic triglyceride. The data are expressed as the mean±SD. *P<0.05 (unpaired t test or ANOVA). **P<0.01.

(Supplementary Fig. 1J–L). Furthermore, compared with the *Atg16l1*$^{fl/fl}$ mice fed the same diet, the *Atg16l1*$^{\Delta M\phi}$ mice fed an HFHCD exhibited a significant increase in visceral adipose tissue inflammation (Supplementary Fig. 1M).

Average food intake and EE were also measured in our study based on the methods of previous studies.[28,29] The body weights of the NCD-fed mice did not significantly differ between the two groups, but a marked increase in body weight was observed in the HFHCD-fed *Atg16l1*$^{\Delta M\phi}$ mice compared with the *Atg16l1*$^{fl/fl}$ mice (Supplementary Fig. 2A). HFHCD-fed *Atg16l1*$^{\Delta M\phi}$ mice consumed significantly less food than *Atg16l1*$^{fl/fl}$ mice (Supplementary Fig. 2B). NCD-fed *Atg16l1*$^{\Delta M\phi}$ mice also consumed significantly less food than *Atg16l1*$^{fl/fl}$ mice (Supplementary Fig. 2C).

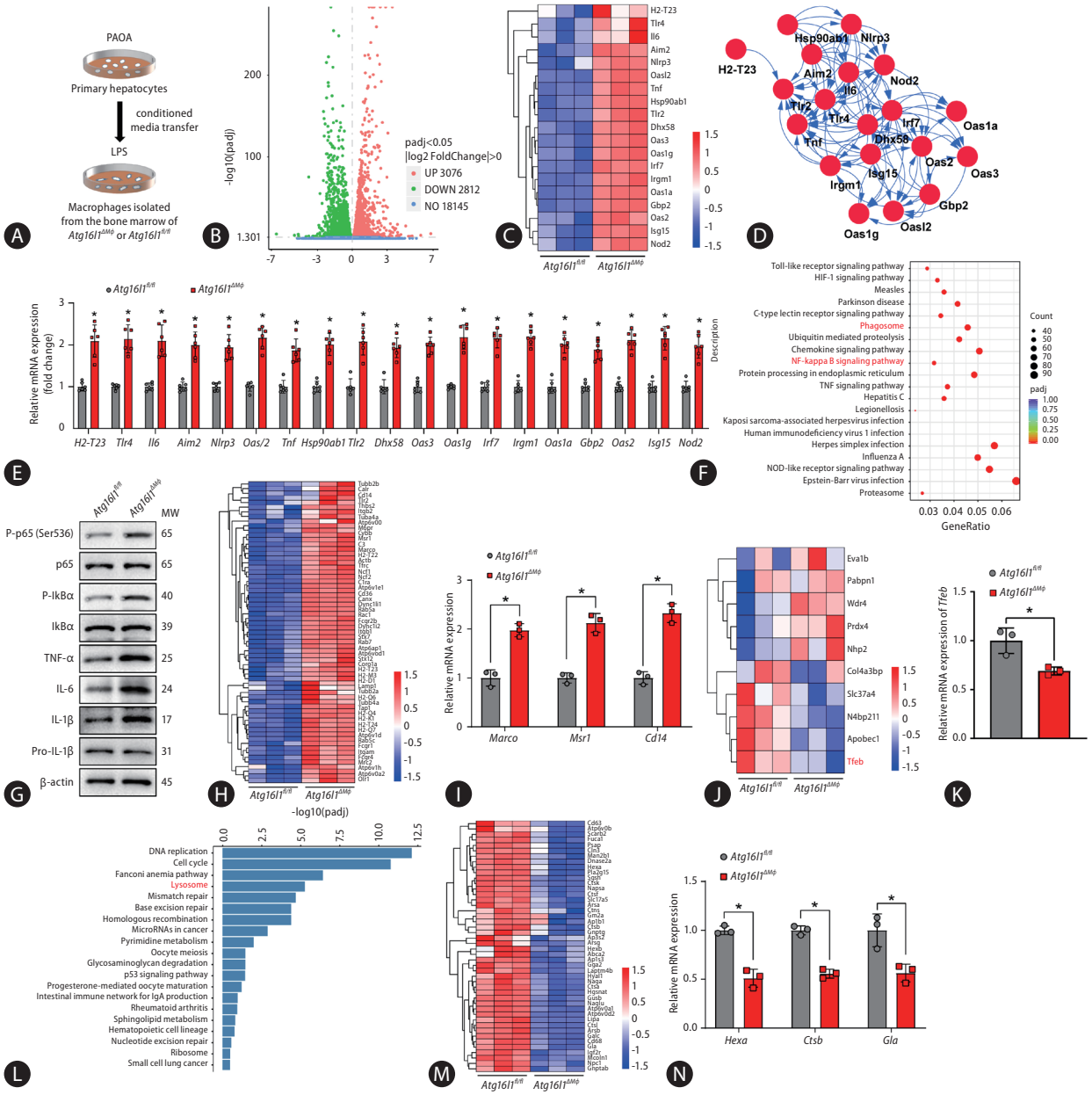

Figure 2. Knockout of macrophage *Atg16l1* expression induces type I interferon signaling and inflammatory responses. (A) Schematic diagram showing that primary hepatocytes isolated from *Atg16l1*$^{fl/fl}$ mice with or without PAOA stimulation were cocultured with LPS-primed primary BMDMs from *Atg16l1*$^{fl/fl}$ and *Atg16l1*$^{\Delta M\phi}$ mice. (B) Volcano plot of all DEGs in cocultured *Atg16l1*$^{fl/fl}$ and *Atg16l1*$^{\Delta M\phi}$ BMDMs. (C) Heatmap showing the clustering of 19 upregulated genes affecting the IFN-I response. (D) STRING-based network analysis of genes detected in (C), revealing a strong contribution of an IFN-I-related signature. (E) The expression of genes detected in (C). (F) KEGG pathway enrichment analysis of the pathways associated with genes whose expression was upregulated in stimulated *Atg16l1*$^{\Delta M\phi}$ BMDMs compared with that in *Atg16l1*$^{fl/fl}$ BMDMs. (G) The proinflammatory protein expression levels in stimulated *Atg16l1*$^{fl/fl}$ and *Atg16l1*$^{\Delta M\phi}$ BMDMs. (H) Heatmap showing the clustering of 65 upregulated genes that affect the phagosome signaling pathway. (I) The gene expression levels of *Marco*, *Msr1*, and *Cd14*. (J) Heatmap showing that *Tfeb* expression was markedly lower in stimulated *Atg16l1*$^{\Delta M\phi}$ BMDMs than in *Atg16l1*$^{fl/fl}$ BMDMs. (K) The gene expression level of *Tfeb* in stimulated *Atg16l1*$^{fl/fl}$ and *Atg16l1*$^{\Delta M\phi}$ BMDMs. (L) KEGG pathway enrichment analysis of the pathways associated with genes whose expression was downregulated in stimulated *Atg16l1*$^{\Delta M\phi}$ BMDMs compared with that in *Atg16l1*$^{fl/fl}$ BMDMs. (M) Heatmap showing the clustering of 46 downregulated genes that affect the lysosome signaling pathway. (N) The gene expression levels of *Hexa*, *Ctsb*, and *Gla*. ATG16L1, autophagy-related protein 16-like 1; PAOA, palmitic acid- and oleic acid; BMDMs, bone marrow-derived macrophages; KEGG, Kyoto Encyclopedia of Genes and Genomes; STING, stimulator of interferon genes. The data are expressed as the mean±SD. *P<0.05 (unpaired t test or ANOVA).

https://doi.org/10.3350/cmh.2024.0107

Moreover, the rates of oxygen consumption (VO_2), CO_2 production (VCO_2), and EE in the *Atg16l1*$^{\Delta M\phi}$ mice were significantly lower than those in the *Atg16l1*$^{fl/fl}$ mice (Supplementary Fig. 2D-F, 2H-J, and 2 L). In contrast, locomotor activity did not significantly differ between the *Atg16l1*$^{\Delta M\phi}$ and *Atg16l1*$^{fl/fl}$ mice (Supplementary Fig. 2G, K). Collectively, these results suggest that ATG16L1 expression is significantly decreased in the liver tissues of mice with MASH and is negatively correlated with MASH development and that macrophage-specific deletion of *Atg16l1* expression exacerbates experimental steatohepatitis.

Macrophage *Atg16l1* knockout induces Type I interferon signaling and the inflammatory response

To further explore the role of ATG16L1 expression in MASH progression, we incubated LPS-primed *Atg16l1*$^{fl/fl}$ or *Atg16l1*$^{\Delta M\phi}$ bone marrow-derived macrophages (BMDMs) with *Atg16l1*$^{fl/fl}$ primary hepatocyte CM for 48 hours (Fig. 2A). Proinflammatory factors were examined, and the results showed that the gene expression and secretion of proinflammatory cytokines were markedly upregulated (Supplementary Fig. 3A, B). By assessing macrophage glycolysis and mitochondrial metabolism, we found that ATG16L1 expression could affect immune responses to MASH by regulating macrophage glycan metabolism. We measured glycolytic and mitochondrial metabolic activity using a Seahorse XFe96 analyzer. The results showed that the level of glycolysis in the *Atg16l1*$^{\Delta M\phi}$ BMDMs was markedly greater than that in the *Atg16l1*$^{fl/fl}$ BMDMs stimulated with CM+LPS (Supplementary Fig. 3C). Moreover, the mitochondrial metabolism level in the *Atg16l1*$^{\Delta M\phi}$ BMDMs was significantly lower than that in the *Atg16l1*$^{fl/fl}$ BMDMs stimulated with CM+LPS (Supplementary Fig. 3D). Next, the treated *Atg16l1*$^{fl/fl}$ or *Atg16l1*$^{\Delta M\phi}$ BMDMs (shown in Fig. 2A) were subjected to RNA sequencing analysis. In total, we identified 5,888 DEGs (Fig. 2B), including 3076 genes with upregulated expression and 2812 genes with downregulated expression (*Atg16l1*$^{\Delta M\phi}$ vs. *Atg16l1*$^{fl/fl}$). The top 19 uniquely upregulated and downregulated genes included the IFN-I–dependent genes *Oas1g*, *Oas3*, *Irgm1*, and *Irf7*, which are known to play a role in innate immunity and the antiviral response (Fig. 2C). Using the STRING database,[30] we performed an interaction analysis of the 19 abovementioned genes, which revealed a densely connected network of known IFN-stimulated genes including the *Oas1g*, *Irf7*, *Oas2*, and *Isg15* genes (Fig. 2D). Moreover, qRT–PCR analysis of these 19 upregulated IFN-stimulated genes confirmed the above findings (Fig. 2E). Next, we performed Kyoto Encyclopedia of Genes and Genomes (KEGG) pathway enrichment analysis according to genotype and treatment, which revealed significant enrichment of upregulated genes related to NF-κB signaling and the phagosome signaling pathway (Fig. 2F). The upregulation of the proinflammatory NF-κB signaling pathway was validated by observation of increased protein expression levels of p-p65 (Ser536), p-IkBα, TNF-α, IL-6, and IL-1β (Fig. 2G). We analyzed the upregulated phagosome signaling pathway and found 65 significantly upregulated phagosome-related genes (Fig. 2H). The increased expression levels of three representative phagosome-related genes, *Marco*, *Mrs1*, and *Cd14*, in activated *Atg16l1*$^{\Delta M\phi}$ BMDMs further confirmed this result (Fig. 2I). Moreover, RNA sequencing and mRNA expression data indicated that the expression of the transcription factor EB (*Tfeb*), a master transcriptional regulator of autophagy and lysosomes,[31] was significantly lower in activated *Atg16l1*$^{\Delta M\phi}$ BMDMs than in activated *Atg16l1*$^{fl/fl}$ BMDMs (Fig. 2J, K). Further analysis of the KEGG pathway enrichment analysis results also revealed significant enrichment of downregulated genes related to lysosomes (Fig. 2L). Next, we analyzed the downregulated lysosome signaling pathway and identified 46 significantly downregulated lysosome-related genes (Fig. 2M). The decreased expression levels of three representative lysosome-related genes, *Hexa*, *Ctsb*, and *Gla*, in activated *Atg16l1*$^{\Delta M\phi}$ BMDMs further validated this result (Fig. 2N). To clarify the above results, we constructed myeloid-specific *Atg16l1* gene knock-in mice (*Atg16l1*^{OE}). The overall expression levels of ATG16L1 in liver tissues or hepatocytes from *Atg16l1*^{OE} and *Atg16l1*$^{fl/fl}$ mice showed no significant difference. BMDMs isolated from *Atg16l1*^{OE} mice showed significantly higher levels of ATG16L1 than those isolated from *Atg16l1*$^{fl/fl}$ mice (Supplementary Fig. 3E). We incubated LPS-primed *Atg16l1*$^{fl/fl}$ or *Atg16l1*^{OE} BMDMs with primary hepatocyte CM from *Atg16l1*$^{fl/fl}$ mice for 48 h (Supplementary Fig. 3F). The expression and secretion of proinflammatory factors were significantly decreased (Supplementary Fig. 3G, H). The level of glycolysis in the *Atg16l1*^{OE} BMDMs was markedly lower than that in the *At-*

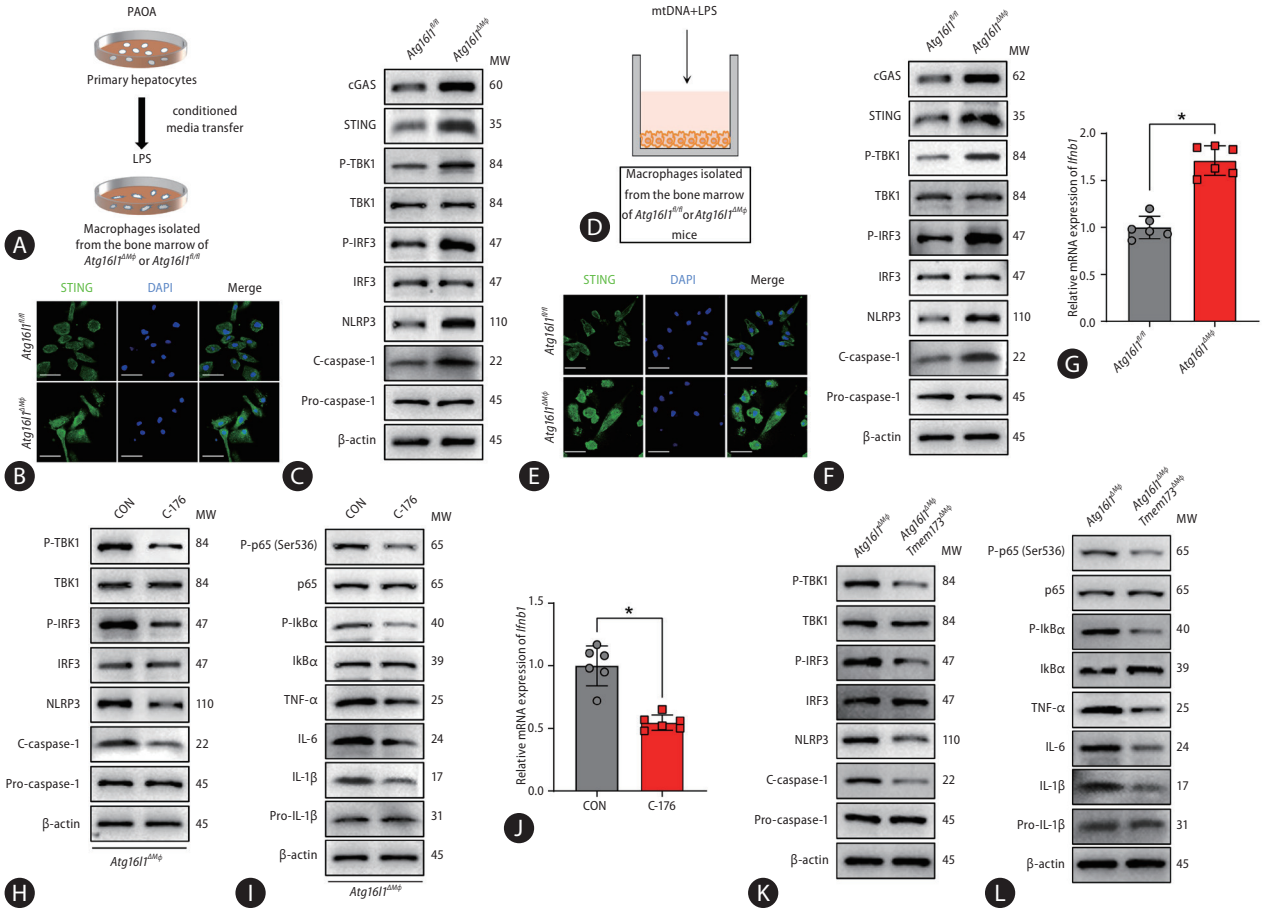

Figure 3. Macrophage *Atg16l1* deficiency promotes the activation of the cGAS/STING pathway. (A) Schematic diagram showing that primary hepatocytes with or without PAOA stimulation isolated from *Atg16l1*$^{fl/fl}$ mice were cocultured with LPS-primed primary BMDMs from *Atg16l1*$^{fl/fl}$ and *Atg16l1*$^{\Delta M\phi}$ mice. (B) Immunofluorescence staining for STING expression in *Atg16l1*$^{fl/fl}$ and *Atg16l1*$^{\Delta M\phi}$ BMDMs. (C) The expression levels of proteins involved in cGAS/STING signaling. (D) Schematic diagram showing that LPS-primed primary BMDMs from *Atg16l1*$^{fl/fl}$ and *Atg16l1*$^{\Delta M\phi}$ mice were cocultured with mtDNA from hepatocytes from HFHCD-fed WT mice. (E) Immunofluorescence staining for STING. (F) The protein expression levels of cGAS/STING signaling markers and (G) the mRNA expression level of *Ifnb1* in stimulated *Atg16l1*$^{fl/fl}$ and *Atg16l1*$^{\Delta M\phi}$ BMDMs treated with mtDNA+LPS. (H) The expression levels of STING signaling proteins, (I) proinflammatory proteins and (J) *Ifnb1* mRNA in (mtDNA+LPS)-stimulated *Atg16l1*$^{\Delta M\phi}$ BMDMs treated with the STING inhibitor C-176. (K) The expression levels of STING signaling-related proteins and (L) proinflammatory proteins in (mtDNA+LPS)-stimulated *Atg16l1*$^{\Delta M\phi}$*Tmem173*$^{\Delta M\phi}$ BMDMs. ATG16L1, autophagy-related protein 16-like 1; PAOA, palmitic acid- and oleic acid; BMDMs, bone marrow-derived macrophages; STING, stimulator of interferon genes. The data are expressed as the mean±SD. *P<0.05 (unpaired t test or ANOVA).

g16l1$^{fl/fl}$ BMDMs stimulated with CM+LPS (Supplementary Fig. 3I), whereas the level of mitochondrial metabolism in the *Atg16l1*^{OE} BMDMs was significantly greater than that in the *Atg16l1*$^{fl/fl}$ BMDMs stimulated with CM+LPS (Supplementary Fig. 3J). Moreover, the expression levels of IFN-related genes were markedly lower in activated *Atg16l1*^{OE} BMDMs than in activated *Atg16l1*$^{fl/fl}$ BMDMs (Supplementary Fig. 3K). Furthermore, the expression levels of proinflammatory proteins in the NF-κB signaling pathway were also lower in activated *Atg16l1*^{OE} BMDMs than in activated *Atg16l1*$^{fl/fl}$ BMDMs (Supplementary Fig. 3L).

Macrophage *Atg16l1* deficiency promotes the activation of the cGAS/STING pathway

A previous study demonstrated that cyclic GMP-AMP synthase (cGAS) synthesizes the dinucleotide secondary messenger 2'3'-cGAMP, which then activates STING, an endoplasmic reticulum-resident adaptor, inducing its traf-

https://doi.org/10.3350/cmh.2024.0107

ficking to the endoplasmic reticulum–Golgi intermediate complex (ERGIC), where TANK-binding kinase 1 (TBK1) phosphorylates the IFN-I-inducing transcription factor interferon regulatory factor 3 (IRF3).[32] Meanwhile, activated IRF3 promotes NLRP3 inflammasome expression.[33] Our results demonstrated that the cGAS/STING signaling pathway was markedly activated in LPS-primed *Atg16l1*$^{\Delta M\phi}$ BMDMs compared with *Atg16l1*$^{fl/fl}$ BMDMs cultured in CM from *Atg16l1*$^{fl/fl}$ primary hepatocytes for 48 hours (Fig. 3A–C).

Our previous study revealed that mitochondrial DNA (mtDNA) released from pyroptotic hepatocytes contributes to STING activation in macrophages.[34] In this study, we also investigated hepatocyte pyroptosis in liver tissues from MASH patients and found that hepatocyte pyroptosis was significantly greater in liver tissues from MASH patients than in those from normal controls, which was confirmed by the increase in Gasdermin D (GSDMD) activation (Supplementary Fig. 4A, B). Furthermore, we examined GSDMD expression in murine MASH model mice and found that GSDMD was significantly activated in hepatocytes isolated from MASH mice, which was reflected by increased levels of GSDMD-N fragments and increased hepatocyte death (Supplementary Fig. 4C, D). As damage-associated molecular pattern molecules (DAMPs) play an important role in the inflammatory response,[35] we examined the levels of DAMPs in hepatocytes isolated from MASH mice. The levels of ATP and mtDNA in the supernatants of pyroptotic hepatocytes isolated from MASH mice were significantly greater than those in the supernatants of control hepatocytes (Supplementary Fig. 4E, F). Next, we isolated mtDNA from pyroptotic hepatocytes (Supplementary Fig. 4G) and stimulated WT BMDMs with isolated mtDNA tagged with Cy5. mtDNA-Cy5 was engulfed by BMDMs at 12 h postcoculture (Supplementary Fig. 4H). Furthermore, CM from palmitic acid- and oleic acid (PAOA)-stimulated hepatocytes was also used to coculture LPS-primed BMDMs with or without the mtDNA scavenger ethidium bromide (EtBr) (Supplementary Fig. 4I). We found that the expression of proinflammatory genes (*Tnfa*, *Il6*, *Il1b*), *Ifnb1*, and *Tgfb1* was significantly decreased in activated BMDMs with mtDNA depletion (Supplementary Fig. 4J–L). Next, mtDNA was isolated from pyroptotic hepatocytes and used to stimulate *Atg16l1*$^{fl/fl}$, *Atg16l1*$^{\Delta M\phi}$ or *Atg16l1*^{OE} BMDMs. mtDNA-Cy5 was more engulfed by the *Atg16l1*$^{\Delta M\phi}$ BMDMs and less engulfed by the *Atg16l1*^{OE} BMDMs at 12 hours postcoculture with mtDNA-Cy5 than by the *Atg16l1*$^{fl/fl}$ BMDMs (Supplementary Fig. 4M).

To explore the key role of mtDNA in regulating the ATG16L1-mediated macrophage immune response, we cocultured BMDMs from *Atg16l1*$^{fl/fl}$ or *Atg16l1*$^{\Delta M\phi}$ mice with mtDNA isolated from pyroptotic hepatocytes (Fig. 3D). The results suggested that the cGAS/STING signaling pathway was markedly activated (Fig. 3E–G) in LPS-primed *Atg16l1*$^{\Delta M\phi}$ BMDMs compared with *Atg16l1*$^{fl/fl}$ BMDMs stimulated with mtDNA. Next, we treated activated *Atg16l1*$^{\Delta M\phi}$ BMDMs with the STING inhibitor C-176 to clarify the important role of STING signaling in ATG16L1-mediated macrophage inflammation. The results showed that the downstream signaling activation of STING was markedly decreased (Fig. 3H–J). Subsequently, we treated *Atg16l1*$^{\Delta M\phi}$*Tmem173*$^{\Delta M\phi}$ BMDMs with mtDNA to clarify the important role of STING signaling in ATG16L1-mediated macrophage inflammation. STING signaling and inflammation were significantly suppressed in the *Atg16l1*$^{\Delta M\phi}$*Tmem173*$^{\Delta M\phi}$ BMDMs compared with the *Atg16l1*$^{\Delta M\phi}$ BMDMs (Fig. 3K, L). Furthermore, we cocultured *Atg16l1*^{OE} BMDMs with CM from PAOA-stimulated hepatocytes or mtDNA from pyroptotic hepatocytes and found that the STING signaling pathway was markedly inhibited in the *Atg16l1*^{OE} BMDMs compared with the *Atg16l1*$^{fl/fl}$ BMDMs (Supplementary Fig. 5A–E). Next, we treated activated *Atg16l1*^{OE} BMDMs with the STING activator DMXAA. The results indicated that STING signaling was upregulated in the opposite manner in the *Atg16l1*^{OE} BMDMs treated with DMXAA (Supplementary Fig. 5F–H). To explore the role of STING in MASH, we constructed MASH model *Atg16l1*$^{\Delta M\phi}$*Tmem173*$^{\Delta M\phi}$ mice. As a result, attenuated MASH was found in *Atg16l1*$^{\Delta M\phi}$*Tmem173*$^{\Delta M\phi}$ mice compared with that in *Atg16l1*$^{\Delta M\phi}$ mice (Supplementary Fig. 6A–F). Furthermore, we also assessed the body weight and energy expenditure of HFHCD-fed *Atg16l1*$^{\Delta M\phi}$*Tmem173*$^{\Delta M\phi}$ mice compared to *Atg16l1*$^{\Delta M\phi}$ mice. The results indicated that HFHCD-fed *Atg16l1*$^{\Delta M\phi}$ *Tmem173*$^{\Delta M\phi}$ mice exhibited decreased body weight compared to *Atg16l1*$^{\Delta M\phi}$ mice, along with increased energy expenditure (Supplementary Fig. 6G, H).

 https://doi.org/10.3350/cmh.2024.0107

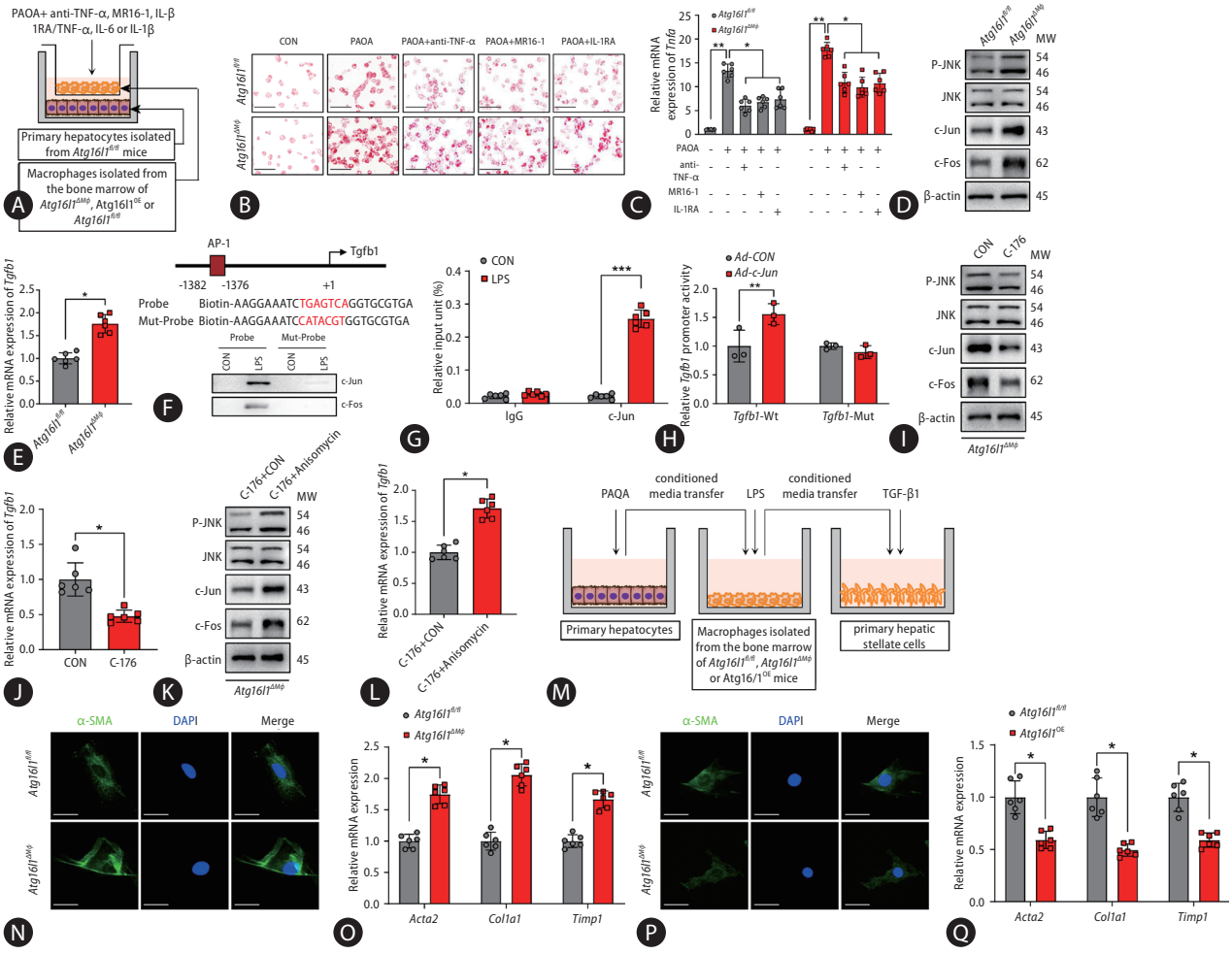

Figure 4. Macrophage *Atg16l1* deficiency induces hepatocyte lipid accumulation and HSC activation. (A) Schematic diagram showing the co-culture of primary hepatocytes from *Atg16l1*$^{fl/fl}$ mice with LPS-primed primary BMDMs from *Atg16l1*$^{fl/fl}$, *Atg16l1*$^{\Delta M\phi}$ and *Atg16l1*^{OE} mice with or without anti-TNF-α, MR16-1, IL-1RA, TNF-α, IL-6 or IL-1β and PAOA treatment. (B) Lipid accumulation determined by oil red O staining and (C) *Tnfa* mRNA expression levels in primary *Atg16l1*$^{fl/fl}$ hepatocytes cocultured with *Atg16l1*$^{fl/fl}$ and *Atg16l1*$^{\Delta M\phi}$ macrophages in PAOA medium with or without anti-TNF-α, MR16-1, or IL-1RA. (D) The protein expression levels of p-JNK, JNK, c-Jun, c-Fos and (E) *Tgfb1* mRNA in LPS-primed *Atg16l1*$^{fl/fl}$ and *Atg16l1*$^{\Delta M\phi}$ macrophages cultured with CM from PAOA-stimulated *Atg16l1*$^{fl/fl}$ hepatocytes. (F) DNA pull-down assay. (G) ChIP assay. (H) Dual-luciferase reporter assay. (I) The protein expression levels of p-JNK, JNK, c-Jun, c-Fos and (J) *Tgfb1* mRNA in LPS-primed *Atg16l1*$^{\Delta M\phi}$ macrophages treated with CM from PAOA-stimulated *Atg16l1*$^{fl/fl}$ hepatocytes with or without stimulation by the STING inhibitor C-176. (K) The protein expression levels of p-JNK, JNK, c-Jun, c-Fos and (L) *Tgfb1* mRNA in LPS-primed *Atg16l1*$^{\Delta M\phi}$ macrophages treated with CM from PAOA-stimulated *Atg16l1*$^{fl/fl}$ hepatocytes treated with C-176 with or without the JNK activator anisomycin. (M) Primary hepatocyte-conditioned media was transferred to LPS-primed *Atg16l1*$^{fl/fl}$, *Atg16l1*$^{\Delta M\phi}$ or *Atg16l1*^{OE} BMDMs for 48 hours, and BMDM-CM was then transferred to primary mouse HSCs in the absence or presence of TGF-β1 (8 ng/mL for 24 hours). (N) Immunofluorescence staining for α-SMA (green) and (O) the *Acta2*, *Col1a1*, and *Timp1* genes in treated primary mouse HSCs. Scale bar, 50 μm. (P) α-SMA (green) immunofluorescence staining and (Q) *Acta2*, *Col1a1*, and *Timp1* gene expression in treated primary mouse HSCs. Scale bar, 50 μm. ATG16L1, autophagy-related protein 16-like 1; HSCs, hepatic stellate cells; BMDMs, bone marrow-derived macrophages; PAOA, palmitic acid- and oleic acid; STING, stimulator of interferon genes. The data are expressed as the mean±SD. *P<0.05, **P<0.01 (unpaired t test or ANOVA). ***P<0.001.

https://doi.org/10.3350/cmh.2024.0107

Knockout of macrophage *Atg16l1* expression promotes hepatocyte lipid accumulation and HSC activation

Next, we determined whether ATG16L1-mediated macrophage inflammation affects lipid metabolism in hepatocytes. We assessed the ability of macrophage-derived TNF-α, IL-6, and IL-1β to induce steatohepatitis and the effectiveness of neutralizing antibodies against these cytokines against steatohepatitis. We used a coculture system of LPS-primed *Atg16l1*$^{\Delta M\phi}$, *Atg16l1*^{OE}, or *Atg16l1*$^{fl/fl}$ macrophages with primary *Atg16l1*$^{fl/fl}$ hepatocytes (Fig. 4A). The neutralizing antibodies against TNF-α, IL-6, or IL-1β, including anti-TNF-α, MR16-1, and IL-1RA, decreased hepatocyte lipid accumulation and inflammation (Fig. 4B, C) in the *Atg16l1*$^{fl/fl}$ hepatocytes cocultured with LPS-primed *Atg16l1*$^{\Delta M\phi}$ macrophages, whereas administration of TNF-α, IL-6, or IL-1β increased lipid deposition (Supplementary Fig. 7A) and inflammatory responses (Supplementary Fig. 7B) in the *Atg16l1*$^{fl/fl}$ hepatocytes cocultured with LPS-primed *Atg16l1*^{OE} macrophages.

A previous study showed that JNK1 activation in macrophages could promote TGF-β1 expression and affect HSC activation.[36] The activation of hepatic JNK1, c-Jun, and AP-1 signaling occurs in parallel with the development of steatohepatitis in MASH mice.[37] We determined the phosphorylation levels of JNK, c-Jun, and c-Fos and found that JNK, c-Jun, and c-Fos phosphorylation was significantly greater in *Atg16l1*$^{\Delta M\phi}$ macrophages than in *Atg16l1*$^{fl/fl}$ macrophages (Fig. 4D). The expression of *Tgfb1* in *Atg16l1*$^{\Delta M\phi}$ macrophages was also greater than that in *Atg16l1*$^{fl/fl}$ macrophages (Fig. 4E). We performed sequence alignment analysis of the *Tgfb1* gene and identified an AP-1 binding site between amino acids -1382 and -1376 in the *Tgfb1* promoter region (Fig. 4F). Based on this information, we performed a DNA pull-down assay to determine whether LPS treatment might alter the association of AP-1 with the *Tgfb1* promoter. We observed that LPS treatment increased the binding of c-Jun and c-Fos to the AP-1 binding site in the *Tgfb1* promoter region (Fig. 4F). Moreover, a chromatin immunoprecipitation (ChIP)-qPCR assay revealed the enrichment of c-Jun at the *Tgfb1* promoter region in response to LPS treatment (Fig. 4G). Next, mutation of the AP-1 binding sites to which c-Jun binds in the *Tgfb1* promoter region abrogated the increase in *Tgfb1* promoter activity triggered by *c-Jun* overexpression (Fig. 4H). We treated activated *Atg16l1*$^{\Delta M\phi}$ BMDMs with the STING inhibitor C-176 and found that the protein expression levels of phosphorylated JNK, c-Jun, and c-Fos and the mRNA expression level of *Tgfb1* were significantly decreased (Fig. 4I, J), whereas the protein expression levels of phosphorylated JNK, c-Jun, and c-Fos and the mRNA expression level of *Tgfb1* were significantly increased when C-176-treated *Atg16l1*$^{\Delta M\phi}$ BMDMs were stimulated with the JNK activator anisomycin (Fig. 4K, L). To confirm the above results, we determined the protein expression levels of phosphorylated JNK, c-Jun, and c-Fos and the mRNA expression level of *Tgfb1* in *Atg16l1*^{OE} BMDMs. The results showed that *Atg16l1* overexpression markedly reduced the expression levels of phosphorylated JNK, c-Jun, and c-Fos and the mRNA expression of *Tgfb1* (Supplementary Fig. 7C, D). Next, we treated activated *Atg16l1*^{OE} BMDMs with the STING activator DMXAA and found that the protein levels of phosphorylated JNK, c-Jun, and c-Fos significantly increased (Supplementary Fig. 7E), whereas the protein expression levels of phosphorylated JNK, c-Jun, and c-Fos significantly decreased when DMXAA-treated *Atg16l1*$^{\Delta M\phi}$ BMDMs were stimulated with the JNK inhibitor SP600125 (Supplementary Fig. 7F). To validate whether macrophage ATG16L1 expression affects HSC activation, we incubated primary mouse HSCs in the absence or presence of TGF-β1 (8 ng/mL) with CM from *Atg16l1*$^{\Delta M\phi}$, *Atg16l1*^{OE} or *Atg16l1*$^{fl/fl}$ BMDMs treated with primary hepatocyte CM from *Atg16l1*$^{fl/fl}$ mice for 24 hours (Fig. 4M). α-SMA immunofluorescence and *Acta2*, *Col1a1*, and *Timp1* gene expression in HSCs indicated that macrophage *Atg16l1* knockout markedly promoted the activation of HSCs, while *Atg16l1* overexpression significantly suppressed HSC activation (Fig. 4N–Q).

Depletion of macrophage *Atg16l1* expression suppresses lipophagy and promotes STING signaling activation

Next, we explored the specific mechanisms underlying the ATG16L1-mediated regulation of the STING signaling pathway in MASH. In yeast and mammalian cells, ATG16L1 is responsible for proper subcellular localization of the autophagy machinery.[38,39] The decreased protein expression level of LC3B and increased protein expression level of

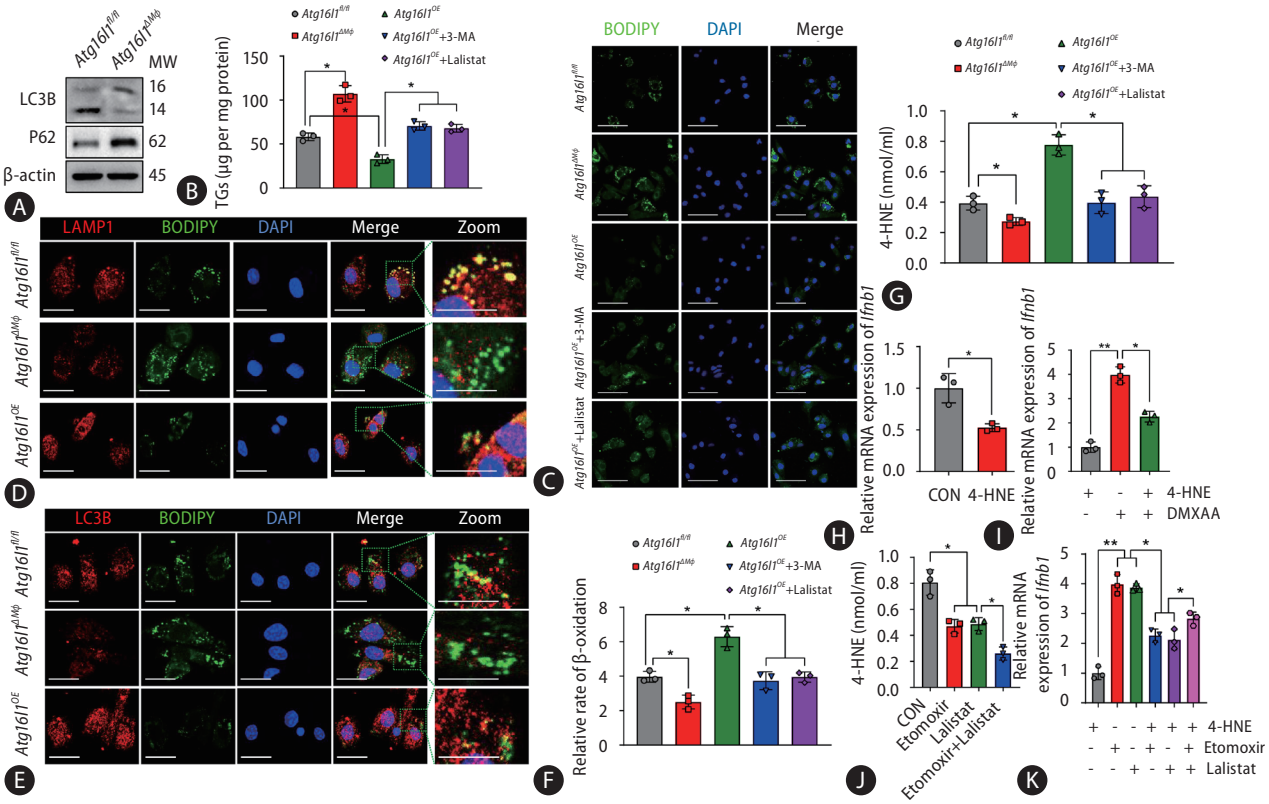

Figure 5. Macrophage *Atg16l1* depletion suppresses lipophagy and promotes STING signaling activation. (A) LC3B and P62 protein levels and (B) TG levels in LPS-primed *Atg16l1*$^{fl/fl}$ and *Atg16l1*$^{\Delta M\phi}$ macrophages cultured with CM from PAOA-stimulated *Atg16l1*$^{fl/fl}$ hepatocytes. (C) BODIPY 493/503 staining of treated macrophages. Scale bar, 50 μm. (D) Colocalization of BODIPY 493/503 (green) staining with LAMP1 (red) expression and (E) BODIPY 493/503 (green) staining with LC3 (red) expression in *Atg16l1*$^{fl/fl}$, *Atg16l1*$^{\Delta M\phi}$, and *Atg16l1*^{OE} macrophages treated with CM from PAOA-stimulated *Atg16l1*$^{fl/fl}$ hepatocytes. Scale bar, 20 μm. (F) The levels of β-oxidation and (G) the levels of 4-HNE in *Atg16l1*$^{fl/fl}$, *Atg16l1*$^{\Delta M\phi}$, and *Atg16l1*^{OE} macrophages treated with CM from PAOA-stimulated *Atg16l1*$^{fl/fl}$ hepatocytes with or without the autophagy inhibitor 3-MA and the LIPA inhibitor lalistat. (H) *Ifnb1* mRNA expression in LPS-primed WT macrophages treated with CM from PAOA-stimulated WT hepatocytes with or without 4-HNE. (I) *Ifnb1* mRNA expression in LPS-primed WT macrophages treated with CM from PAOA-stimulated WT hepatocytes with or without 4-HNE and DMXAA. (J) 4-HNE levels in activated WT macrophages treated with the β-oxidation inhibitor etomoxir. (K) *Ifnb1* mRNA expression in LPS-primed WT macrophages treated with CM from PAOA-stimulated WT hepatocytes with or without 4-HNE and etomoxir. (L) Immunoblot analysis of STING carbonylation by selective labeling with *m*-APA in WT BMDMs treated with 4-HNE (6.4 μM) or (M) in activated *Atg16l1*$^{fl/fl}$, *Atg16l1*$^{\Delta M\phi}$, and *Atg16l1*^{OE} BMDMs. (N) Immunoblot analysis of STING palmitoylation by click chemistry in WT BMDMs pre-treated with 4-HNE following DMXAA stimulation or (O) in activated *Atg16l1*$^{fl/fl}$, *Atg16l1*$^{\Delta M\phi}$, and *Atg16l1*^{OE} BMDMs. (P) Confocal analysis of the co-localization of STING (green) expression and expression of the cis-Golgi protein GM130 (red) in LPS-primed *Atg16l1*$^{fl/fl}$, *Atg16l1*$^{\Delta M\phi}$, and *Atg16l1*^{OE} BMDMs with or without CM from PAOA-stimulated *Atg16l1*$^{fl/fl}$ hepatocytes. Scale bar, 10 μm. ATG16L1, autophagy-related protein 16-like 1; STING, stimulator of interferon genes; PAOA, palmitic acid- and oleic acid; CM, conditioned media. The data are expressed as the mean±SD. **P*<0.05, ***P*<0.01 (unpaired t test or ANOVA).

p62 in the *Atg16l1*$^{\Delta M\phi}$ BMDMs suggested that *Atg16l1* knockout markedly suppressed autophagy (Fig. 5A), while the increased protein expression level of LC3B and decreased protein expression level of p62 in the *Atg16l1*^{OE} BMDMs suggested that *Atg16l1* overexpression markedly promoted autophagy (Supplementary Fig. 8A). We found that the inhibition of lipophagy led to increased lipid accumulation, as evidenced by the elevated TG (Fig. 5B), BODIPY 493/503 (Fig. 5C), oil red O (Supplementary Fig. 8B), and lipid droplet levels in BMDMs, as visualized by electron microscopy (Supplementary Fig. 8C). Previous studies indicated that lipophagy, i.e., the autophagy of lipid droplets (LDs),[40] plays an important role in regulating cellular lipid metabolism.[41] Thus, we hypothesized that ATG16L1 promotes lipophagy and thereby decreases cellular lipid accumulation. Autophagy is characterized by the formation

https://doi.org/10.3350/cmh.2024.0107

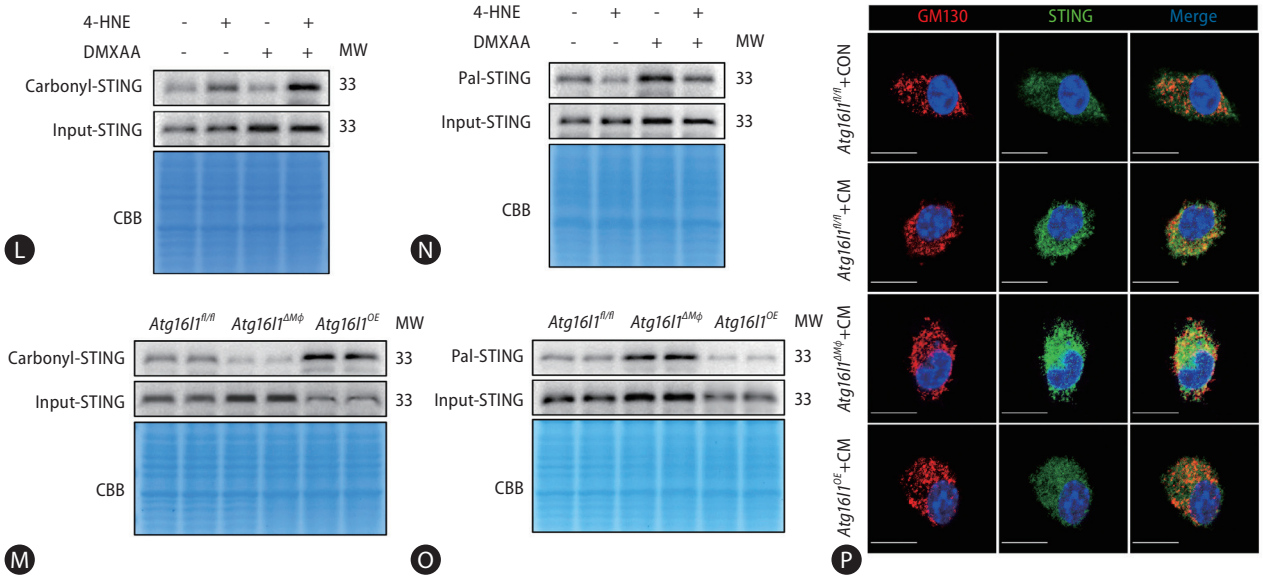

Figure 5. Continued.

of autophagosomes, which deliver cytoplasmic material to lysosomes.[42] To confirm that lysosomes regulate intracellular lipid levels, the effect of lysosomal hydrolysis on lipid stores was examined. Dual immunofluorescence studies revealed increased colocalization of LDs with lysosome-associated membrane protein 1 (LAMP1) in LPS-primed and CM-treated *Atg16l1*$^{fl/fl}$ BMDMs; *Atg16l1* deletion inhibited lysosomal hydrolysis of lipid stores, whereas *Atg16l1* overexpression promoted lysosomal hydrolysis of lipid stores (Fig. 5D). Furthermore, LD colocalization with the autophagosome marker LC3 demonstrated a direct association between LDs and autophagosomes, supporting a constitutive function for autophagy in regulating LDs (Fig. 5E). Electron microscopy was used to verify LD degradation by autophagic lysosomes (Supplementary Fig. 8D). A previous study indicated that the inhibition of autophagy decreases TG β-oxidation.[38] Our study also demonstrated that *Atg16l1* knockout decreased macrophage β-oxidation, whereas *Atg16l1* overexpression increased β-oxidation (Fig. 5F). A recent study demonstrated that lipid peroxidation promoted the production of 4-hydroxynonenal (4-HNE), which is the major end product of lipid peroxidation. Increased 4-HNE production enhanced STING carbonylation, resulting in the inhibition of STING trafficking from the endoplasmic reticulum to the Golgi apparatus and the suppression of STING activation.[43] We also examined cellular 4-HNE levels and revealed that *Atg16l1* knockout decreased 4-HNE production, whereas *Atg16l1* overexpression increased 4-HNE production (Fig. 5G). Another study showed that peroxisomal β-oxidation acted as a sensor for intracellular fatty acid levels and regulated lipolysis.[44] Our study demonstrated that the presence of 4-HNE suppressed the mRNA expression of *Ifnb1* (Fig. 5H, I). Moreover, the inhibition of lipophagy and β-oxidation decreased the production of 4-HNE and increased the mRNA expression of *Ifnb1* (Fig. 5J, K). In addition, 4-HNE induced STING carbonylation (Fig. 5L and Supplementary Fig. 8E), *Atg16l1* knockout inhibited STING carbonylation, and *Atg16l1* overexpression promoted STING carbonylation (Fig. 5M). Study has indicated that the palmitoylation of STING was crucial for the IFN I response in macrophages, but it didn't affect the translocation of STING.[45] Our results indicated that 4-HNE blocked STING palmitoylation (Fig. 5N), *Atg16l1* knockout promoted STING palmitoylation, and *Atg16l1* overexpression inhibited STING palmitoylation (Fig. 5O). The trafficking of STING from the ER to the Golgi apparatus is a crucial step for STING activation and subsequent IRF3 activation.[32] To investigate STING trafficking from the ER to the Golgi apparatus in the context of differential ATG16L1 expression, we costained for STING and the Golgi marker GM130 in LPS-primed *Atg16l1*$^{fl/fl}$, LPS-primed and CM-treated *Atg16l1*$^{fl/fl}$, LPS-primed and CM-treated *Atg16l1*$^{\Delta M\phi}$, and LPS-primed and CM-treated *Atg16l1*^{OE} BMDMs (Fig. 5P). The results showed that

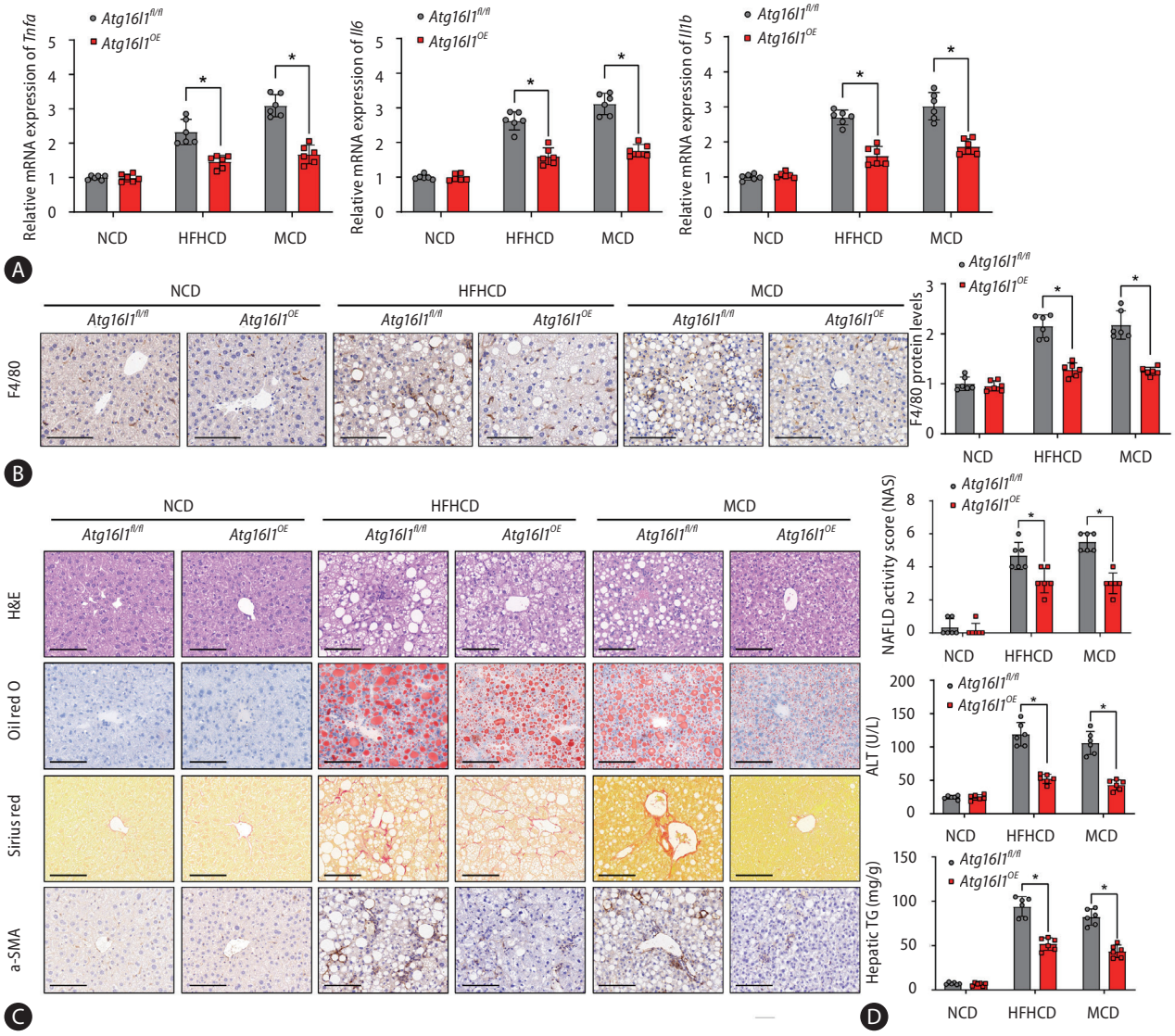

Figure 6. Macrophage *Atg16l1* overexpression ameliorates the progression of experimental steatohepatitis. Hepatic *Tnfa*, *Il6*, and *Il1b* gene expression in *Atg16l1*$^{fl/fl}$ and *Atg16l1*^{OE} MASH mice. (B) Hepatic F4/80^{+} cell immunohistochemistry. (C) Representative hepatic H&E staining, oil red O staining, Sirius Red staining, and α-SMA immunohistochemical analysis. (D) NAS, serum ALT levels, and hepatic TG levels; n=6/group. (E) Hepatic *Acta2*, *Col1a1* and *Timp1* gene expression levels; n=6 mice/group. (F) Hepatic α-SMA, collagen-I, and TIMP-1 protein expression levels. (G, H) Representative photographs of the livers, BAT, eWAT, and ingWAT of the *Atg16l1*$^{fl/fl}$ and *Atg16l1*^{OE} mice fed an HFHCD. MASH, metabolic dysfunction-associated steatohepatitis; ATG16L1, autophagy-related protein 16-like 1; NAS, NAFLD activity score; ALT, alanine aminotransferase; BAT, brown adipose tissue; eWAT, epididymal white adipose tissue; ingWAT, inguinal white adipose tissue; HFHCD, high-fat and high-cholesterol diet. The data are expressed as the mean±SD. **P*<0.05 (unpaired t test or ANOVA).

macrophage ATG16L1 depletion promoted STING localization to the Golgi apparatus, whereas ATG16L1 overexpression inhibited STING localization to the Golgi apparatus. Furthermore, compared to *Atg16l1*$^{fl/fl}$ MASH mice, liver tissues of *Atg16l1*$^{\Delta M\phi}$ MASH mice exhibited impaired autophagy and activation of the STING signaling pathway, indicated by upregulation of protein expression levels of P62, cGAS, Pal-STING, P-TBK1, and P-IRF3, along with downregulation of protein expression levels of LC3B and Carbonyl-STING (Supplementary Fig. 8F).

https://doi.org/10.3350/cmh.2024.0107

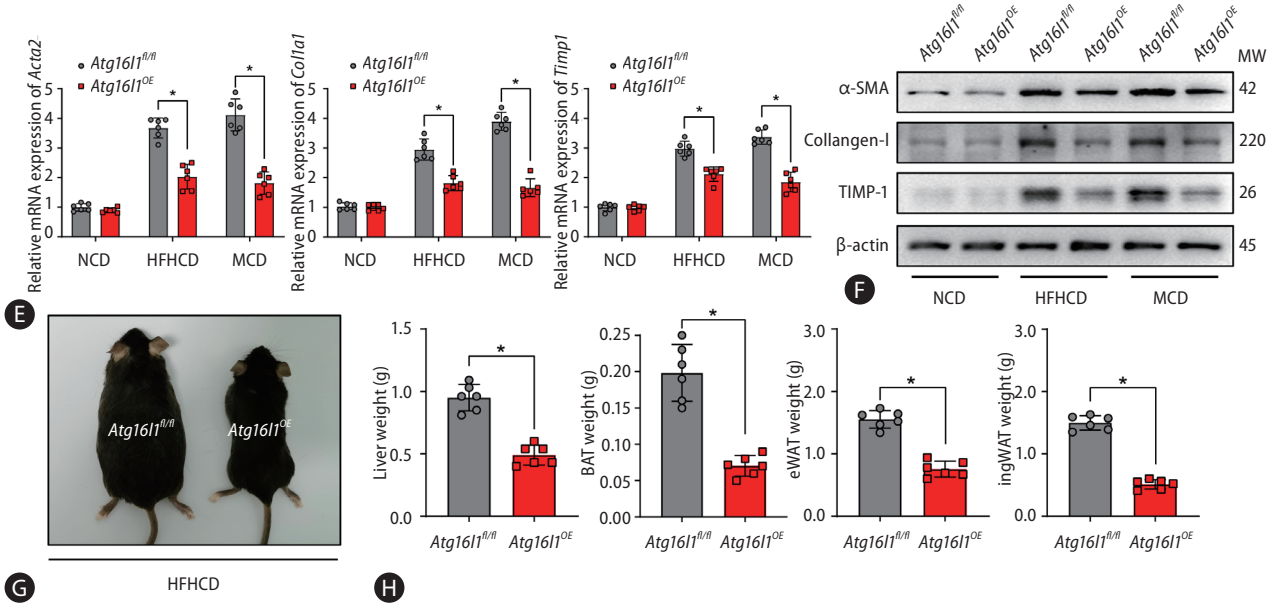

Figure 6. Continued.

Macrophage *Atg16l1* overexpression ameliorates the progression of experimental steatohepatitis

Next, *Atg16l1*^{OE} mice and *Atg16l1*$^{fl/fl}$ mice were bred and fed an HFHCD for 16 weeks or an MCD for 6 weeks. Macrophage *Atg16l1* overexpression decreased proinflammatory gene expression (Fig. 6A) and macrophage infiltration (Fig. 6B). Histopathology of liver sections demonstrated that *Atg16l1*^{OE} mice had improved liver histology and less steatosis and inflammation than *Atg16l1*$^{fl/fl}$ mice (Fig. 6C). Accordingly, the levels of serum ALT and hepatic TG were significantly lower in the *Atg16l1*^{OE} mice than in the *Atg16l-1*$^{fl/fl}$ mice (Fig. 6D). Moreover, *Atg16l1*^{OE} mice exhibited significantly mitigated liver fibrosis, as indicated by decreased Sirius red and α-SMA staining (Fig. 6C); decreased expression levels of the profibrotic genes *Acta2*, *Col1a1* and *Timp1*; and decreased protein expression levels of α-SMA, collagen-I, and TIMP-1 (Fig. 6E, F). Moreover, compared to *Atg16l1*$^{fl/fl}$ mice, liver tissues of *Atg16l1*^{OE} mice exhibited enhanced autophagy and suppression of the STING signaling pathway, indicated by decreased protein expression levels of P62, cGAS, Pal-STING, P-TBK1, and P-IRF3, along with increased protein expression levels of LC3B and Carbonyl-STING (Supplementary Fig. 8G). The weights of tissues, including livers, BAT, eWAT and ingWAT, of the *Atg16l1*^{OE} mice fed an HFHCD were lower than those of the *Atg16l1*$^{fl/fl}$ mice fed the same diet (Fig. 6G, H).

The body weights and fat masses of the NCD-fed mice were not significantly different between the two genotypes, but we observed a marked decrease in weight gain driven by fat mass in the HFHCD-fed *Atg16l1*^{OE} mice (Supplementary Fig. 9A). Furthermore, there was no significant difference between the amount of food consumed by HFHCD-fed *Atg16l1*^{OE} mice and that consumed by *Atg16l1*$^{fl/fl}$ mice (Supplementary Fig. 9B). Similarly, there was no significant difference between the amount of food consumed by the NCD-fed *Atg16l1*^{OE} mice and that consumed by the *Atg16l1*$^{fl/fl}$ mice (Supplementary Fig. 9C). Nevertheless, the rates of VO_2, VCO_2, and EE in the *Atg16l1*^{OE} mice were significantly greater than those in the *Atg16l1*$^{fl/fl}$ mice (Supplementary Fig. 9D-F, 9H-J, 9L). In contrast, locomotor activity did not significantly differ between the *Atg16l1*^{OE} and *Atg16l1*$^{fl/fl}$ mice (Supplementary Fig. 9G, K). Collectively, these results suggest that *Atg16l1* overexpression in macrophages ameliorates steatohepatitis in mice.

Pharmacological enhancement of ATG16L1 expression prevents MASH development

Finally, we explored the effects of pharmacologically induced ATG16L1 overexpression on steatohepatitis progres-

 https://doi.org/10.3350/cmh.2024.0107

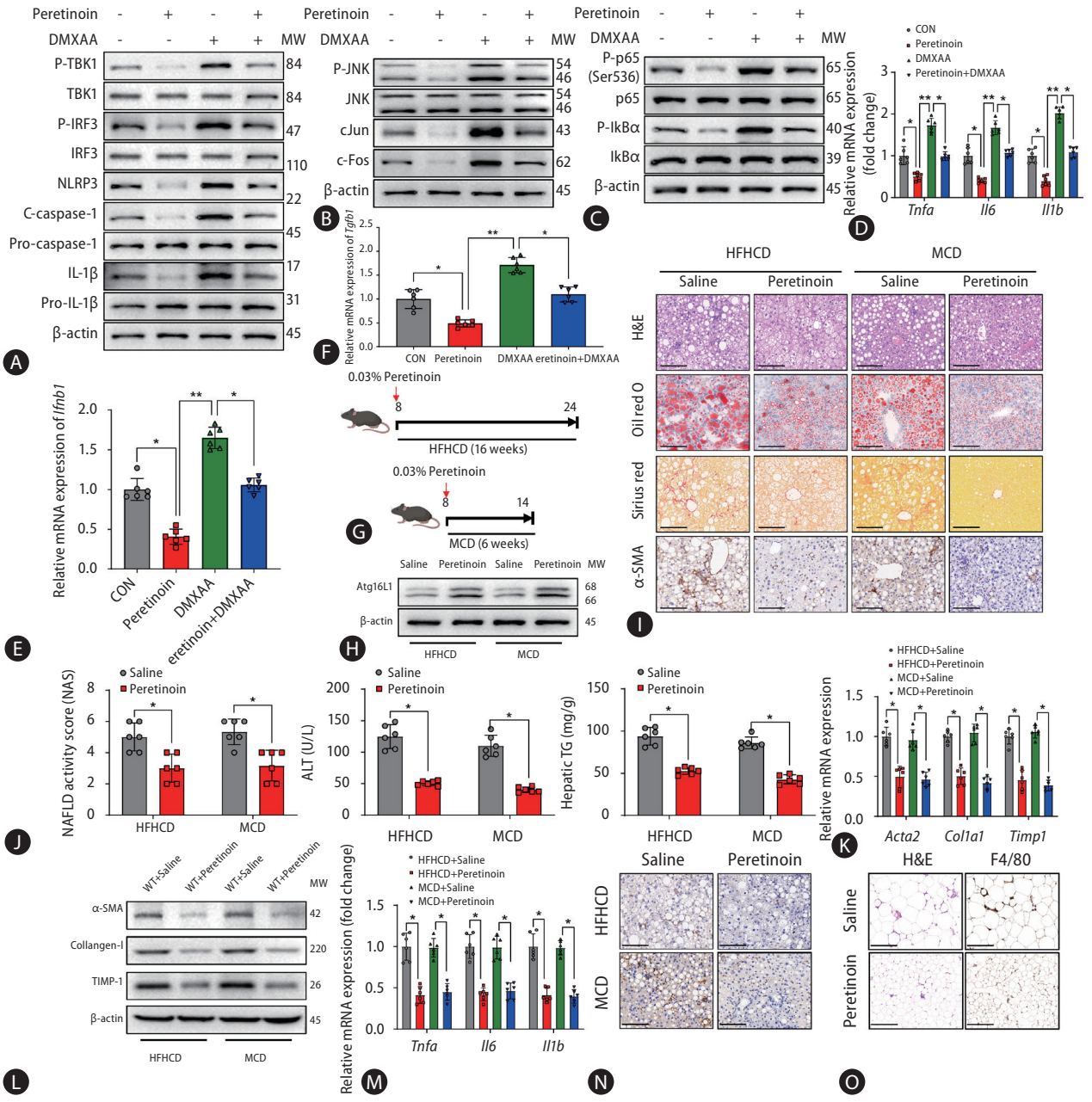

Figure 7. Pharmacological enhancement of ATG16L1 expression prevents MASH development. The protein expression levels of STING signaling components in activated WT BMDMs treated with CM from PAOA-stimulated hepatocytes with or without the ATG16L1 enhancer peretinoin following DMXAA stimulation. (B) The protein levels of p-JNK, JNK, c-Jun, and c-Fos in activated WT BMDMs treated with CM. (C) The proinflammatory protein expression levels, (D) proinflammatory gene expression levels, and (E) *Ifnb1* and (F) *Tgfb1* mRNA expression in activated WT BMDMs treated with CM. (G) Schematic representation of HFHCD-fed or MCD-fed WT mice supplemented with dietary peretinoin. (H) Hepatic ATG16L1 protein expression levels. (I) Hepatic H&E staining, oil red O staining, Sirius red staining, and α-SMA immunohistochemistry. (J) NAS, serum ALT levels, and hepatic TG levels. (K) Hepatic *Acta2*, *Col1a1*, and *Timp1* gene expression; n=6 mice/group. (L) Hepatic α-SMA, collagen-I, and TIMP-1 protein expression levels. (M) Hepatic *Tnfa*, *Il6*, and *Il1b* gene expression levels. (N) Hepatic F4/80^{+} cell immunohistochemistry. (O) Representative eWAT H&E staining and F4/80 immunohistochemistry image of HFHCD-fed WT mice treated with or without peretinoin. MASH, metabolic dysfunction-associated steatohepatitis; ATG16L1, autophagy-related protein 16-like 1; BMDMs, bone marrow-derived macrophages; STING, stimulator of interferon genes; PAOA, palmitic acid- and oleic acid; CM, conditioned media; HFHCD, high-fat and high-cholesterol diet; MCD, methionine- and choline-deficient diet; NAS, NAFLD activity score; ALT, alanine aminotransferase; TG, hepatic triglyceride; eWAT, epididymal white adipose tissue. The data are expressed as the mean±SD. *P<0.05, **P<0.01 (unpaired t test or ANOVA).

https://doi.org/10.3350/cmh.2024.0107

sion. An ATG16L1 enhancer (peretinoin) was used to treat activated WT BMDMs stimulated with or without DMXAA. The results showed that increased ATG16L1 protein expression levels inhibited STING signaling pathway activation, decreased the expression of phosphorylated JNK, c-Jun, and c-Fos, and suppressed macrophage inflammation and *Tgfb1* expression (Fig. 7A–F). Moreover, peretinoin was added to the diets of WT mice fed an HFHCD for 16 consecutive weeks or fed an MCD for 6 consecutive weeks (Fig. 7G). Peretinoin treatment increased ATG16L1 protein expression levels in liver tissues from MASH mice (Fig. 7H). Histopathology of liver sections revealed that compared with untreated mice fed the same diet, WT MASH mice treated with peretinoin had improved liver histology with markedly reduced steatosis, inflammation, and fibrosis markers (Fig. 7I). Accordingly, the levels of serum ALT and hepatic TG were significantly lower in WT MASH mice treated with peretinoin than in untreated mice fed the same diet (Fig. 7J). Similar results were found regarding the gene and protein expression levels of profibrotic markers (Fig. 7K, L). Moreover, proinflammatory gene expression and macrophage infiltration were significantly lower in WT MASH mice treated with peretinoin than in untreated mice fed the same diet (Fig. 7M, N). Furthermore, compared with untreated mice fed the same diet, HFHCD-fed WT mice treated with peretinoin exhibited a significant decrease in visceral adipose tissue inflammation (Fig. 7O).

To further validate the role of macrophage ATG16L1 in MASH, we also treated *Atg16l1*$^{\Delta M\phi}$ mice and *Atg16l1*$^{fl/fl}$ mice with peretinoin in the MCD-induced MASH model. Histopathology of liver sections revealed that compared with untreated group, the MASH phenotype in *Atg16l1*$^{\Delta M\phi}$ mice treated with peretinoin showed slight improvement, with mild reductions in markers of steatosis, inflammation, and fibrosis. However, it was more severe than in *Atg16l1*$^{fl/fl}$ mice treated with peretinoin (Supplementary Fig. 10A). We speculate that peretinoin might also partially by promoting ATG16L1 expression in hepatocytes and other cell types to ameliorate MASH, which deserved further exploration in our future study. Accordingly, serum ALT and liver TG levels in *Atg16l1*$^{\Delta M\phi}$ mice treated with peretinoin were lower than untreated *Atg16l1*$^{\Delta M\phi}$ mice, but higher than peretinoin-treated *Atg16l1*$^{fl/fl}$ mice (Supplementary Fig. 10B). Additionally, profibrotic and proinflammatory genes also exhibited similar outcomes (Supplementary Fig. 10C, D). These results demonstrate that pharmacological enhancement of ATG16L1 protein expression levels alleviates steatohepatitis and fibrosis in mice.

DISCUSSION

Herein, we identified macrophage ATG16L1 expression as a novel inhibitor of MASH. In vivo studies demonstrated that macrophage-specific *Atg16l1* knockout exacerbates MASH, whereas transgenic overexpression of *Atg16l1* attenuates MASH in mice. Moreover, we found that *Atg16l1* knockout decreased EE, whereas *Atg16l1* overexpression increased EE. Further experiments showed that *Atg16l1* knockout suppressed macrophage lipophagy, which subsequently suppressed macrophage β-oxidation and decreased 4-HNE production. Decreased 4-HNE levels inhibited STING carbonylation, promoted STING palmitoylation and induced STING trafficking from the ER to the Golgi apparatus and the activation of downstream STING signaling, thereby increasing proinflammatory and profibrotic cytokine secretion, resulting in hepatocyte steatosis and HSC activation. Furthermore, *Atg16l1* expression deficiency promoted macrophage phagocytosis but impaired lysosomal activity, increasing the amount of mtDNA released by pyroptotic hepatocytes. Increased mtDNA abundance activated macrophage cGAS/STING signaling. Pharmacological ATG16L1 overexpression alleviated MASH progression in mice. Thus, macrophage ATG16L1 represents a promising therapeutic target for MASH treatment.

In mammalian cells, ATG16L1 is responsible for proper subcellular localization of the autophagic machinery.[40] A previous study indicated that the induction of autophagy may ameliorate hepatic steatosis, and siRNA-mediated ATG16L1 expression knockdown resulted in increased lipid accumulation.[46] However, the specific mechanisms underlying ATG16L1-mediated regulation of MASH remain unknown. Although decreased *Atg16L1* mRNA expression was found in the livers of patients with MASH based on markers of disease progression,[17] the specific mechanisms underlying ATG16L1-mediated regulation of MASH remain unknown.

A previous study showed that hepatic macrophages might become activated due to excess lipid accumulation

and defective lipid processing.[47] Therefore, more studies are needed to explore effective methods to promote macrophage LD degradation in MASH. Another study indicated that autophagy might promote the β-oxidation of triglycerides.[41] Our study revealed that impaired lipophagy in macrophages suppressed macrophage β-oxidation and decreased the production of the lipid peroxidation end product 4-HNE. *Atg16l1* knockout decreased EE, whereas *Atg16l1* overexpression increased EE in mice with MASH. Macrophage-specific *Atg16l1* depletion exacerbates steatohepatitis development by suppressing macrophage lipophagy.

Moreover, a previous study showed that impaired ATG16L1 expression enhances monocyte phagocytosis in Crohn's disease patients.[48] Our study revealed that *Atg16l1* knockout enhances macrophage phagocytosis by increasing the amount of mtDNA released by pyroptotic hepatocytes. STING is a critical integrator that acts in response to stimulation via cGAMP produced by cGAS and has a fundamental role in the induction of innate immune responses triggered by the presence of cytosolic DNA.[43] STING activation is vital for host defense against viral infection and for the mediation of DNA damage-induced inflammation. In the resting state, STING localizes to the ER, and the Ca^{2+} sensor stromal interaction molecule 1 facilitates its retention to enforce immunological quiescence.[49] After engagement with cGAMP or other cyclic dinucleotides, STING is activated and moves from the ER to the Golgi apparatus,[50] where it induces IRF3 activation, type I IFN expression, and the inflammatory response. Thus, STING trafficking from the ER to the Golgi apparatus is a key step in signal activation. Previous studies have reported that STING expression is increased in liver tissues from MASH patients and promotes macrophage-mediated hepatic inflammation and fibrosis in mice.[36,21] Another study indicated that lipid peroxidation led to STING carbonylation via the lipid peroxidation end product 4-HNE and inhibited STING trafficking from the ER to the Golgi complex.[43] Therefore, STING signaling plays an important role in MASH development. Our study confirmed that macrophage-specific *Atg16l1* depletion exacerbates MASH development by suppressing macrophage lipophagy, which subsequently suppresses macrophage β-oxidation and decreases the production of 4-HNE. Decreased 4-HNE levels inhibited STING carbonylation, enhanced STING palmitoylation, and promoted STING trafficking from the ER to the Golgi apparatus, which subsequently maintained downstream STING signaling activation.

In summary, we revealed the role of ATG16L1 expression in MASH. Macrophage-specific *Atg16l1* knockout exacerbates the development of steatohepatitis by suppressing macrophage lipophagy, which subsequently suppresses macrophage β-oxidation and decreases the production of 4-HNE. Decreased 4-HNE levels enhanced STING palmitoylation, which ultimately promoted the secretion of proinflammatory and profibrotic cytokines, resulting in hepatocyte steatosis and HSC activation. Transgenic *Atg16l1* overexpression in macrophages reversed the above results. These results indicate that targeting ATG16L1 expression might be promising for the management of steatohepatitis.

Authors' contributions

QW, QB, ZX, HZ, and LL participated in the research design. LL and HZ supervised the study. QW, QB, ZX, HZ, and LL drafted the manuscript. QW, QB, ZX, YL, JZ, and YP conducted the experiments. All the authors have read and approved the final manuscript.

Acknowledgements

This work was supported by grants from the National Natural Science Foundation of China (81971495, 82370668, 82071798), the CAMS Innovation Fund for Medical Sciences (No. 2019-I2M-5-035) and the Postgraduate Research & Practice Innovation Program of Jiangsu Province (KYCX24_2030).

Conflicts of Interest

The authors have no conflicts to disclose.

SUPPLEMENTARY MATERIAL

Supplementary material is available at Clinical and Molecular Hepatology website (http://www.e-cmh.org).

REFERENCES

1. Younossi Z, Anstee QM, Marietti M, Hardy T, Henry L, Eslam M,

et al. Global burden of NAFLD and NASH: trends, predictions, risk factors and prevention. Nat Rev Gastroenterol Hepatol 2018;15:11-20.
2. Rinella ME, Lazarus JV, Ratziu V, Francque SM, Sanyal AJ, Kanwal F, et al. A multisociety Delphi consensus statement on new fatty liver disease nomenclature. J Hepatol 2023;79:1542-1556.
3. Kleiner DE, Brunt EM, Van Natta M, Behling C, Contos MJ, Cummings OW, et al. Design and validation of a histological scoring system for nonalcoholic fatty liver disease. Hepatology 2005;41:1313-1321.
4. Loomba R, Friedman SL, Shulman GI. Mechanisms and disease consequences of nonalcoholic fatty liver disease. Cell 2021;184:2537-2564.
5. Spengler EK, Loomba R. Recommendations for diagnosis, referral for liver biopsy, and treatment of nonalcoholic fatty liver disease and nonalcoholic steatohepatitis. Mayo Clin Proc 2015;90:1233-1246.
6. Wong VW, Chitturi S, Wong GL, Yu J, Chan HL, Farrell GC. Pathogenesis and novel treatment options for non-alcoholic steatohepatitis. Lancet Gastroenterol Hepatol 2016;1:56-67.
7. Mizushima N, Levine B, Cuervo AM, Klionsky DJ. Autophagy fights disease through cellular self-digestion. Nature 2008;451:1069-1075.
8. Shintani T, Klionsky DJ. Autophagy in health and disease: a double-edged sword. Science 2004;306:990-995.
9. Weiskirchen R, Tacke F. Relevance of Autophagy in parenchymal and non-parenchymal liver cells for health and disease. Cells 2019;8:16.
10. Tacke F. Targeting hepatic macrophages to treat liver diseases. J Hepatol 2017;66:1300-1312.
11. Lodder J, Denaës T, Chobert MN, Wan J, El-Benna J, Pawlotsky JM, et al. Macrophage autophagy protects against liver fibrosis in mice. Autophagy 2015;11:1280-1292.
12. Gual P, Gilgenkrantz H, Lotersztajn S. Autophagy in chronic liver diseases: the two faces of Janus. Am J Physiol Cell Physiol 2017;312:C263-C273.
13. Allaire M, Rautou PE, Codogno P, Lotersztajn S. Autophagy in liver diseases: time for translation? J Hepatol 2019;70:985-998.
14. Gilgenkrantz H, Mallat A, Moreau R, Lotersztajn S. Targeting cell-intrinsic metabolism for antifibrotic therapy. J Hepatol 2021;74:1442-1454.
15. Matsuzawa-Ishimoto Y, Hwang S, Cadwell K. Autophagy and inflammation. Annu Rev Immunol 2018;36:73-101.
16. Li Y, Sha Y, Wang H, He L, Li L, Wen S, et al. Intracellular C3 prevents hepatic steatosis by promoting autophagy and very-low-density lipoprotein secretion. FASEB J 2021;35:e22037.
17. Okada H, Takabatake R, Honda M, Takegoshi K, Yamashita T, Nakamura M, et al. Peretinoin, an acyclic retinoid, suppresses steatohepatitis and tumorigenesis by activating autophagy in mice fed an atherogenic high-fat diet. Oncotarget 2017;8:39978-39993.
18. Wang Q, Zhou H, Bu Q, Wei S, Li L, Zhou J, et al. Role of XBP1 in regulating the progression of non-alcoholic steatohepatitis. J Hepatol 2022;77:312-325.
19. Zhou H, Wang H, Ni M, Yue S, Xia Y, Busuttil RW, et al. Glycogen synthase kinase 3β promotes liver innate immune activation by restraining AMP-activated protein kinase activation. J Hepatol 2018;69:99-109.
20. Koh EH, Yoon JE, Ko MS, Leem J, Yun JY, Hong CH, et al. Sphingomyelin synthase 1 mediates hepatocyte pyroptosis to trigger non-alcoholic steatohepatitis. Gut 2021;70:1954-1964.
21. Yu Y, Liu Y, An W, Song J, Zhang Y, Zhao X. STING-mediated inflammation in Kupffer cells contributes to progression of non-alcoholic steatohepatitis. J Clin Invest 2019;129:546-555.
22. Loomba R, Noureddin M, Kowdley KV, Kohli A, Sheikh A, Neff G, et al. Combination therapies including cilofexor and firsocostat for bridging fibrosis and cirrhosis attributable to NASH. Hepatology 2021;73:625-643.
23. Brasaemle DL, Rubin B, Harten IA, Gruia-Gray J, Kimmel AR, Londos C. Perilipin A increases triacylglycerol storage by decreasing the rate of triacylglycerol hydrolysis. J Biol Chem 2000;275:38486-38493.
24. Hoppel C, DiMarco JP, Tandler B. Riboflavin and rat hepatic cell structure and function. Mitochondrial oxidative metabolism in deficiency states. J Biol Chem 1979;254:4164-4170.
25. Kaushik S, Massey AC, Cuervo AM. Lysosome membrane lipid microdomains: novel regulators of chaperone-mediated autophagy. EMBO J 2006;25:3921-3933.
26. Huai W, Song H, Yu Z, Wang W, Han L, Sakamoto T, et al. Mint3 potentiates TLR3/4- and RIG-I-induced IFN-β expression and antiviral immune responses. Proc Natl Acad Sci U S A 2016;113:11925-11930.
27. Chao CC, Ma YS, Stadtman ER. Modification of protein surface hydrophobicity and methionine oxidation by oxidative systems. Proc Natl Acad Sci U S A 1997;94:2969-2974.
28. van der Klaauw AA, Croizier S, Mendes de Oliveira E, Stadler LKJ, Park S, Kong Y, et al. Human semaphorin 3 variants link melanocortin circuit development and energy balance. Cell

2019;176:729-742.e18.
29. Ko MS, Yun JY, Baek IJ, Jang JE, Hwang JJ, Lee SE, et al. Mitophagy deficiency increases NLRP3 to induce brown fat dysfunction in mice. Autophagy 2021;17:1205-1221.
30. Szklarczyk D, Jensen LJ. Protein-protein interaction databases. Methods Mol Biol 2015;1278:39-56.
31. Chao X, Wang S, Zhao K, Li Y, Williams JA, Li T, et al. Impaired TFEB-mediated lysosome biogenesis and autophagy promote chronic ethanol-induced liver injury and steatosis in mice. Gastroenterology 2018;155:865-879.e12.
32. Dobbs N, Burnaevskiy N, Chen D, Gonugunta VK, Alto NM, Yan N. STING activation by translocation from the ER is associated with infection and autoinflammatory disease. Cell Host Microbe 2015;18:157-168.
33. Li N, Zhou H, Wu H, Wu Q, Duan M, Deng W, et al. STING-IRF3 contributes to lipopolysaccharide-induced cardiac dysfunction, inflammation, apoptosis and pyroptosis by activating NLRP3. Redox Biol 2019;24:101215.
34. Liu Z, Wang M, Wang X, Bu Q, Wang Q, Su W, et al. XBP1 deficiency promotes hepatocyte pyroptosis by impairing mitophagy to activate mtDNA-cGAS-STING signaling in macrophages during acute liver injury. Redox Biol 2022;52:102305.
35. Garcia-Martinez I, Shaker ME, Mehal WZ. Therapeutic opportunities in damage-associated molecular pattern-driven metabolic diseases. Antioxid Redox Signal 2015;23:1305-1315.
36. Luo X, Li H, Ma L, Zhou J, Guo X, Woo SL, et al. Expression of STING is increased in liver tissues from patients with NAFLD and promotes macrophage-mediated hepatic inflammation and fibrosis in mice. Gastroenterology 2018;155:1971-1984.e4.
37. Schattenberg JM, Singh R, Wang Y, Lefkowitch JH, Rigoli RM, Scherer PE, et al. JNK1 but not JNK2 promotes the development of steatohepatitis in mice. Hepatology 2006;43:163-172.
38. Cadwell K, Liu JY, Brown SL, Miyoshi H, Loh J, Lennerz JK, et al. A key role for autophagy and the autophagy gene Atg16l1 in mouse and human intestinal Paneth cells. Nature 2008;456:259-263.
39. Kuma A, Mizushima N, Ishihara N, Ohsumi Y. Formation of the approximately 350-kDa Apg12-Apg5.Apg16 multimeric complex, mediated by Apg16 oligomerization, is essential for autophagy in yeast. J Biol Chem 2002;277:18619-18625.
40. Qian H, Chao X, Williams J, Fulte S, Li T, Yang L, et al. Autophagy in liver diseases: a review. Mol Aspects Med 2021;82:100973.
41. Singh R, Kaushik S, Wang Y, Xiang Y, Novak I, Komatsu M, et al. Autophagy regulates lipid metabolism. Nature 2009;458:1131-1135.
42. Thoen LF, Guimarães EL, Dollé L, Mannaerts I, Najimi M, Sokal E, et al. A role for autophagy during hepatic stellate cell activation. J Hepatol 2011;55:1353-1360.
43. Jia M, Qin D, Zhao C, Chai L, Yu Z, Wang W, et al. Redox homeostasis maintained by GPX4 facilitates STING activation. Nat Immunol 2020;21:727-735.
44. Ding L, Sun W, Balaz M, He A, Klug M, Wieland S, et al. Peroxisomal β-oxidation acts as a sensor for intracellular fatty acids and regulates lipolysis. Nat Metab 2021;3:1648-1661.
45. Mukai K, Konno H, Akiba T, Uemura T, Waguri S, Kobayashi T, et al. Activation of STING requires palmitoylation at the Golgi. Nat Commun 2016;7:11932.
46. Li R, Guo E, Yang J, Li A, Yang Y, Liu S, et al. 1,25(OH)2 D3 attenuates hepatic steatosis by inducing autophagy in mice. Obesity (Silver Spring) 2017;25:561-571.
47. Remmerie A, Scott CL. Macrophages and lipid metabolism. Cell Immunol 2018;330:27-42.
48. Wolfkamp SC, Verseyden C, Vogels EW, Meisner S, Boonstra K, Peters CP, et al. ATG16L1 and NOD2 polymorphisms enhance phagocytosis in monocytes of Crohn's disease patients. World J Gastroenterol 2014;20:2664-2672.
49. Srikanth S, Woo JS, Wu B, El-Sherbiny YM, Leung J, Chupradit K, et al. The Ca2+ sensor STIM1 regulates the type I interferon response by retaining the signaling adaptor STING at the endoplasmic reticulum. Nat Immunol 2019;20:152-162.
50. Ishikawa H, Ma Z, Barber GN. STING regulates intracellular DNA-mediated, type I interferon-dependent innate immunity. Nature 2009;461:788-792.